METHANE VMR AND CLIMATOLOGY OF AEROSOLS OVER TROPICAL LATITUDES FROM REMOTE SOUNDERS

By

Wondimu Alemu

SUBMITTED IN PARTIAL FULFILLMENT OF THE
REQUIREMENTS FOR THE DEGREE OF
MASTER OF SCIENCE IN PHYSICS
AT
ADDIS ABABA UNIVERSITY
ADDIS ABABA, ETHIOPIA
FEBRUARY 2009

ADDIS ABABA UNIVERSITY

DEPARTMENT OF

PHYSICS

Supervisor: _____

Dr. Gizaw Mengistu

Examiner: _____

Prof. A. V. Gholap

ADDIS ABABA UNIVERSITY

Date: **February 2009**

Author: **Wondimu Alemu**

Title: **Methane VMR and climatology of Aerosols over tropical latitudes from remote sounders**

Department: **Physics**

Degree: **M.Sc.** Convocation: **February** Year: **2009**

Permission is herewith granted to Addis Ababa University to circulate and to have copied for non-commercial purposes, at its discretion, the above title upon the request of individuals or institutions.

Signature of Author

Table of Contents

List of Figures

Abstract

The knowledge of the tropospheric concentration distribution of atmospheric trace gases such as methane and of its temporal evolution allows us to understand chemical processes controlling the atmospheric composition and to estimate the potential contribution of each gas to the climate forcing of the Earth-atmosphere system. Equally, aerosols play an important role in the climate system; the effect of aerosols on the global climate system is one of the major uncertainties of present climate predictions. They play a major role in atmospheric chemistry and hence affect the concentrations of other potentially harmful atmospheric constituents. We have extracted and characterized the volume mixing ratio(VMR) of methane over the equatorial region from the spectral records of ground-based high spectral resolution of FTIR. For this work, the spectral data from the FTIR measurement campaign in October and November 1996 over the Atlantic Ocean covering the region of our study have been used. The retrieval result has given good quality of methane VMR over most of the regions. But unhealthy enhancement is seen in the regions 20^0 South which is attributed to the poor quality of inputs. In addition, comparison of VMR data of Halogen Occultation Experiment (HALOE) satellite with our retrieved VMR data from FTIR has confirmed good agreement over most of the latitude covered by this study and slight discrepancy at certain latitude. With respect to aerosols, the SAGE II instrument has collected vertical profiles of stratospheric and tropospheric aerosol extinction at four wavelengths with high resolution since the program's inception in October, 1984. We extracted the aerosol parameter; the aerosol extinction coefficients derived from version 6.20 series of twenty one years data to characterize the aerosol climatology

of Africa. Accordingly, from monthly mean extinction profile, we have seen a large value of aerosol concentration over troposphere of the Northern, Southern and Eastern regions. Unlike the other two above mentioned regions a large value of aerosol is observed in the lower stratosphere of Eastern region. These cloud of aerosol extinction coefficient is observed at the end of winter and during the summer season of the respective region.

Acknowledgements

I am deeply indebted to Dr. Gizaw Mengistu, my supervisor, for his many suggestions and constant support and friendly approach during this research. His tireless follow up and his consistent support will be in my memory forever. Especially, I highly praise him for his encouragement of independent learning and his facilitation towards research experience gaining from foreign research centers and clearing ways to further education. I should also praise Bahir Dar University for covering educational fees and paying salary for the entire time of my graduate study. My strongest thank is addressed to my mother, Abebech Tsegaye, who lived for myself. She is the hero of my success with out her push and support, this stage would never have come true. I have derived materials from many research journals and books, and am indebted to the authors of those publications and books. I am also thankful to Geletaw Behailu for his patient support in collecting and sending me my salary for entire time.

The second part of this thesis is sponsored by African Laser Center (ALC) and the data and most of the supervision has been provided by Prof Venkataraman Sivakumar, Principal Researcher National Laser Centre (NLC), Council for Scientific and Industrial Research(CSIR). And I was recommended to join the LIDAR project by Dr. Gizaw Mengistu. So it is my greatest pleasure to address my heartiest thank to ALC, Prof. Venkataraman Sivakumar and Dr. Gizaw Mengistu. I am also happy to acknowledge NLC for providing material and facilitating my stay in the CSIR.

Introduction

Remote Sensing is the science and art of acquiring information (spectral, spatial, and temporal) about material objects, area, or phenomenon, without coming into physical contact with the objects, or area, or phenomenon under investigation. In remote sensing, the information is usually derived from capturing electromagnetic radiation (EMR) that is emitted, reflected, absorbed, or scattered in a way that reveals something about the object or scene of interest. This energy may be of natural origin, such as sunlight, star, moon, or it may be artificial, such as radar or laser scanning. Energy can be detected and recorded by photographic film and digital detectors, while more sophisticated radio frequency receivers, radar systems, thermal sensors, radio meters, and other sensing instruments are required for other wavelengths and imaging regimes.

Most remote sensing devices record information about an object by measuring an object's transmission of electromagnetic energy from reflecting and radiating surfaces. For earth and atmospheric parameters, remote sensing is based on measuring radiation which contains the signature of the required characteristics and constituents of the atmosphere (temperature, pressure, concentration of absorbing gases, aerosols and cloud) or of the surface (temperature, moisture, surface wind stress, canopy, etc...).

Active Remote Sensing uses a radiation source generated by artificial means e.g., lasers used for LIDAR or microwaves used in RADAR. Generally a beam of radiation is sent out and a backscattered signal is measured, although it would also be possible to have the source and receiver located at different places. Range-gating enables the user to determine the location of scatterers. Passive Remote Sensing uses natural radiation sources such as the sun, moon, star and the emission of the earth and atmosphere itself. Thus, wavelengths of the solar spectrum from the UV to the IR are accessible and thermal emission by the earth atmosphere system is available from about 4 μm to the far infrared and microwave region.

The advent of ground based instruments and satellites is allowing the acquisition of global and synoptic detailed information about the planets (including the Earth) and their environments. Sensors on Earth-Orbiting satellites provide information about the global patterns and dynamics of clouds, surface vegetation cover and its seasonal variations, surface morphologic structures, ocean surface temperature, gas and particle concentration in the atmosphere, and near-surface wind. The rapid wide coverage capability of satellite platforms allows monitoring of rapidly changing phenomena, particularly in the atmosphere. The long duration and repetitive capability allows the observation of seasonal, annual, and longer-term changes such as polar ice cover, desert expansion, and tropical deforestation. The wide-scale synoptic coverage allows the observation and study regional and continental-scale features such as plate boundaries and mountain chains. Whenever direct measurements of the quantity we are interested are difficult or expensive, remote measurements are used, although they

often bring in their wake complex problems of interpretation generally are known as inverse problems. The atmosphere is typical subject for which remote measurements are cost effective and for which inverse methods are required. The inverse problem is the question of finding the best representation of the required parameters, understanding and describing the information content of a given measurement made, together with any appropriate a priori information that may be available about the system and the measuring device. Inverse theory refers to the inversion of complicated functions regardless of whether the measurement is physically remote, and the problem discussed is inverse problem.

This thesis composed two parts: the first part will present the overall work on the retrieval of methane VMR from the spectral records of FTIR spectrometry and the second part will focus on the climatology of aerosols over Africa as measured by SAGE II. The basics reason to develop climatology of Africa is to validate LIDAR of NLC-CSIR Pretoria, South Africa. This will be presented in the second part of the thesis. The common concepts for both works such as radiative transfer theory and inversion theory are discussed as part of the first work. But it is also directly adopted for the second work so as to avoid repetitions.

Chapter 1

Introduction

1.1 The Earth's atmosphere, composition and structure

The atmosphere of our planet is composed of a group of nearly permanent gases and a group of gases with variable concentrations. In addition, the atmosphere contains various suspended solid and liquid particles mixture, cloud, water drops and ice crystals, precipitations which are variable in space and time.

In general the composition of the atmosphere varies significantly. Carbon dioxide, water and Ozone dominate the interaction with electromagnetic radiation. Moreover, methane and a number of other minor earth's constituents play a role in the Earth's upper atmospheric chemistry [1]. The atmospheric density decreases with altitude, as result the pressure decreases with altitude. In reality the temperature profile is significantly more complex; its value varies vertically and horizontally, depending on the kind of surface, atmospheric constituents their interactions with EM-radiation having specific spectral characteristic. This temperature profile complexity is more in higher altitudes, but in lower atmosphere the temperature does decrease linearly

with altitude at a rate of 6.5 $^oK/km$.

Permanent gas constituents	% by volume
N_2	78.08
O_2	20.94
CO_2	0.934
Ne	0.03
H_2O	0-0.04
O_3	0-12x 10^{-4}
CH_4	0.5x $10-4$

Table 1.1 The earth's atmosphere gases composition

Also present, in quantities less than 1 % by volume are in order: Ar, He, NO_2, CO, NH_3, and others [2]. The major controls upon the composition of the atmosphere and the cycling of these compounds are interactions with the Earths biosphere (living matter) and lithosphere (rock and geological processes such as volcanism). To Describe the interaction of the earth's atmosphere with solar radiation, it is essential that the atmospheric composition is understood [3]. Five layers of the atmosphere have been characterized on account of their thermal characteristics, chemical composition, density and dynamics.

The lower atmosphere, below about 15 km altitude, is termed troposphere because of its turbulent air motions. A boundary layer of about 1 km thickness is often envisaged as an interface between the earth's surface and the free troposphere. The troposphere is characterized by a general decrease in temperature with height, from 15 ^oC at the surface to -50 ^oC at about 15 km. Above this, in the lower stratosphere, the temperature increases with height, the changeover region being known as the

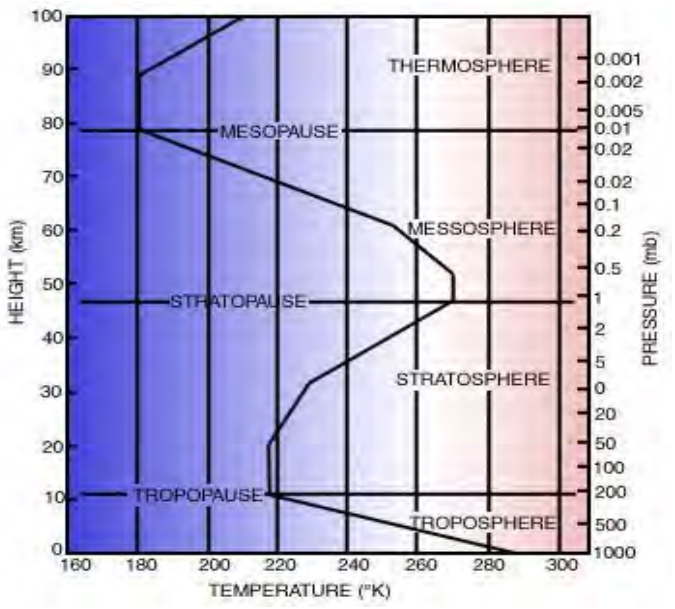

Figure 1.1: Layers of the Earth's atmosphere

tropopause. Troposphere contains an enormous range of inorganic and organic trace substances. Many of them, such as methane, nitrous oxide, dimethyl sulphide, are released by natural processes.

The stratosphere extends from the tropopause up to about 50 km. This layer holds 19 % of the atmospheric gases but the water vapor content is about 1000 times smaller than in the troposphere. Temperature profiles in the stratosphere increases with height due to the ozone layer that absorbs solar ultraviolet (UV) radiation. The top of the stratosphere (stratopause) has temperatures of about 270 K, which is almost the same as the ground level temperature. Above this, the temperature decreases with height.

Mesosphere is a layer extending from approximately 50 km to 80 km, is characterized

by decreasing temperatures, which reach 190-180 ^0K at an altitude of 80 km. In this region, concentrations of ozone and water vapor are negligible. Hence the temperature is lower than that of the troposphere or stratosphere. With increasing distance from Earth's surface the chemical composition of air becomes strongly dependent on altitude and the atmosphere becomes enriched with lighter gases.

Thermosphere extends from 80-85 km to about 640 km. The temperature here increases with height. In the lowest layer of the thermosphere CO_2 is photolyzed to yield CO, resulting in CO concentrations of more than 60 ppm (parts per million), which is 1000 times greater than the values in the troposphere.

All life on earth depends on this atmosphere, but despite this knowledge, humans are altering the atmospheric composition. The emissions from the burning of fossil fuels, from industrial sources such as cement manufacture, and from deforestation are changing the make-up of our atmosphere. In addition, trace gases such as methane and a complex of artificially-produced gases collectively called chlorofluorocarbons (CFCs and HCFCs) are having an impact on the atmosphere wholly out of proportion to their concentration [4].

1.2 Background and motivation

In recent years a growing consensus is emerging that human activities on our planet are contributing to climate change. In order to understand the chemical and physical processes that govern atmospheric balance and to assess the anthropological impact on climate, it is essential to determine the distributions of atmospheric constituents

and to monitor these distributions on a long-term global basis. Atmospheric constituents interact with electromagnetic radiation all across the visible and infrared region as a result of vibrational and rotational process, this impinging their" fingerprints" on the spectral signature of the radiation emitted or scattered toward space [1].

Fourier Transform Infrared Spectroscopy(FTIR) has been found to be one of the most suitable instruments for the measurements of atmospheric trace gases. So measurements from ground-based instruments such as FTIR and satellites can give detailed information about the composition of atmosphere. Many determinations of atmospheric constituents are made from observations of radiance spectra of scattered, reflected and absorbed sunlight (UV, visible and near infrared) or from attenuated thermal emission spectra (infrared and beyond to radio waves). Because the interaction of electromagnetic radiation with matter modifies the incident wave to some extent. The medium therefore produces a signature in the amplitude, phase or spectral composition which depends on composition and structure of the medium [3].

The identification of atmospheric constituent is usually based on detecting the presence of a spectral line or lines associated with a certain molecule. The spectral signature is in effect the "finger print" of a gaseous constituent [1].

The greatest interest of focus is the selective absorption of radiation by atmospheric gases. Molecular absorption is a quantum physics phenomenon involving discrete transfer of energy to excited quantum states; the frequencies of such transitions are

characteristic for each molecule. In the infrared, molecular excitation states are vibrational and rotational; transitions show up as sharply defined lines which often occur in groups (bands)[5]. The strength or intensity of these lines is an indication of the opacity of the atmosphere; a great deal of information about molecular abundances can be deduced from high-resolution measurements taken over such absorption bands. A primary requirement for interpretation of the observed data is the availability of radiative transfer models capable of calculating the observed radiation for realistic atmospheric and observational conditions, and inversions programs for retrieval of vertical temperature and gas concentration profiles.

The retrieval process will generate estimates of a number of atmospheric parameter distributions which together constitute the state vector of parameters to be retrieved. The retrieval is the formal inverse of the forward problem Y = F(X), where Y is the vector of synthetic measurements and F is a function describing the attenuation of solar and/or thermal emission radiation in the atmosphere by means of absorption, scattering and reflection of light. For such retrievals of such atmospheric states, we have used inversion (retrieval) algorithm SFIT-2 software, jointly developed at the NASA Langley Research Center, the National Center for Atmospheric Research (NCAR) and the National Institute Water and Atmosphere Research (NIWA) at Lauder, New Zealand [6]. SFIT-2 is the algorithm used to analyze high-resolution FTIR spectra, which is based on the optimal estimation method (OEM) and allows extracting and characterizing information on the vertical distribution of many FTIR target gases. Retrieval algorithms requires the radiative transfer equation for modeling the observed radiance in addition to measured radiance to derive atmospheric

state parameters. This function is specified by a radiative transfer model. Radiative transfer theory (RT) employed in remote sensing application needs to describe the interaction between matter and electromagnetic radiation.

Optimal estimation theory provides a method for estimating the state of the atmosphere on the basis of priori knowledge (usually a climatological profile), the set of measurements made by the instrument and spectroscopic data extracted from HITRAN [7]. In general, the problem does not have a unique solution so an optimal solution from a number of possible solution is selected.

For the past decade, we have been hearing about how rising levels of greenhouse gases - mainly carbon dioxide, but also methane, nitrous oxide, and the chlorofluorocarbons - will lead to global warming. Thus, it is vital to investigate and understand the current atmospheric constituents such as methane and aerosols.

Methane is the most abundant greenhouse gas in the troposphere after water and carbon dioxide, meaning that its presence in the atmosphere affects the Earth's temperature and climate system [8]. It is, the second most important anthropogenic greenhouse gas, directly contributing $0.48 Wm^{-2}$ to the total anthropogenic radiative forcing of $2.43 Wm^{-2}$ by well-mixed green house gases [9]. CH_4 absorbs the rising radiation from the earth atmosphere system on the near infrared spectral range and play an important role in the greenhouse effect and in the climatic change over the globe [10]. Methane is not toxic below the lower explosive limit of 5% (50000pm). However, when methane is present at high concentrations, it act as an asphyxiant.

Asphyxiants displace oxygen in the air and can cause symptoms of oxygen deprivation (asphyxiation). Changes in the emissions of these species can cause long-term changes in the atmospheric composition and global chemical change. Therefore, a good knowledge of the distribution of these trace gases is necessary to fully understand their role in the atmospheric chemistry.

Aerosol particles are a largely natural, though highly variable, component of our atmosphere. They may be created by wind blowing over dusty regions, by evaporation of sea spray, and by the conversion into tiny particles of some of the gases emitted by plants (Volcanoes may inject large amounts of gases and particles into the stratosphere). Human agricultural and industrial activities add more aerosols, for example through mechanical processes, or by slash-and-burn agricultural practices and increased desertification. However, it is the emission of sulphur dioxide from the burning of coal which has aroused most recent concern. While some of this ends up as acid rain, itself a major environmental problem, a large fraction is converted into sulphate aerosols. Aerosols affect our environment at the local, regional, and global levels. At the local level, aerosols are now becoming recognized as a significant health problem, especially in regard to respiratory illnesses, including asthma. Aerosols can also have a significant impact on visibility and air quality, with potential economic consequences for tourism, cloud formation, meteorology, and climate. Aerosol Particles 0.2-1 μm in diameter that contain sulfate, nitrate, and organic carbon scatter light efficiently. Aerosol particles smaller than 1 μm that contain carbon absorb light efficiently. Aerosol absorption and scattering affect:

1. Radiative energy fluxes, which affect temperature, and

2. Photolysis which affects the composition of the atmosphere.

Aerosol particles also serve as sites on which cloud drops form. In fact, without aerosol particles, clouds would rarely form in the atmosphere. Finally, aerosol particles serve as sites on which chemical reactions take place and as sites for trace gases to condense upon or dissolve within. Thus aerosol should be considered as a part of understanding towards atmospheric chemistry.

The final goal of this work is to understand the abundance of methane by determining its volume mixing ratio over the atmosphere of tropical latitude by using the spectral records of FTIR and to develop climatology of aerosols via the climatology of aerosol extinction coefficient over Africa from the SAGE-II satellite data thereby validate the LiDar of NLC. The first introductory chapter has given an overview of the earth's atmosphere and the overall task of this thesis. The second chapter gives a general information about methane. The detailed discussion on the interaction of Electromagnetic field with gaseous molecule and short look at radiative transfer theory is presented on chapter three. The inversion methods and retrieval theory will be discussed in chapter four. Chapter five gives the retrieval inputs such as spectral microwindows, the FTIR spectral data and a perior used to retrieve methane VMR. The historical understanding of aerosols, properties, its sources and roles in climate change will be discussed in chapter six. Chapter seven presents the description of SAGE-II satellite and the aerosols parameter retrieving method. Finally, the remaining last two chapters will present, results and discussions, lidar validation and conclusion respectively.

Chapter 2

Methane

2.1 Introduction

Methane was determined to be a component of the Earth's atmosphere in 1948 by the analysis of high resolution solar absorption spectra [10]. It is single naturally produced organic present in the largest concentration in the ambient air throughout the world [11] and have molecular structure as shown in Fig 2.1 [12].

Methane is released as a result of both natural as well as human induced activities. Figs 2.3 and 2.4 show the break up of individual sources of methane into the atmosphere. Anthropogenic emissions of methane arise from biogenic sources related to agriculture and waste disposal, including enteric fermentation, animal and human wastes, rice paddies [13], biomass burning, and landfills. Methane is also emitted by the extraction of fossil fuels such as natural gas, coal mining and petroleum. Methane is emitted naturally by wetlands, termites, other wild ruminants, oceans, and hydrates.

Since direct systematic measurements of its trend did not begin until 1978, most of

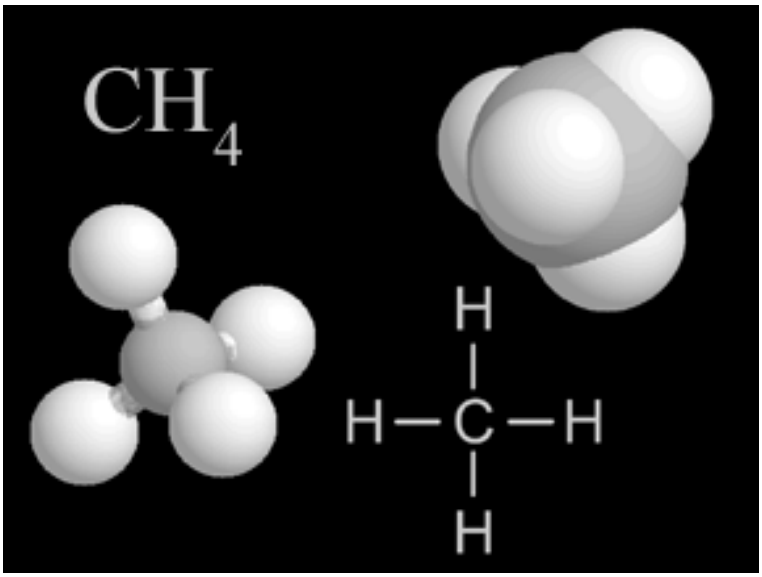

Figure 2.1: Four representations chemists use for methane

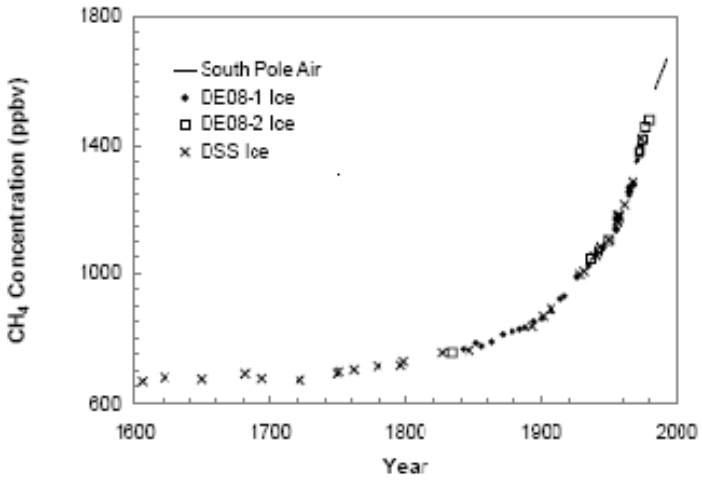

Figure 2.2: Trend of the concentration of Methane

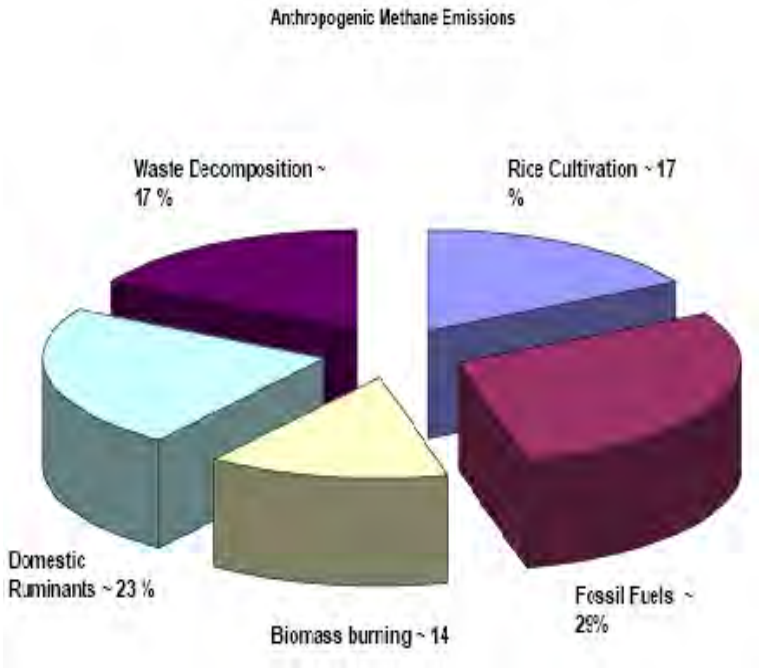

Figure 2.3: Anthropogenic Methane Emissions

the data containing the record of atmospheric CH_4 for earlier times, are obtained by analyzing bubbles of ancient air preserved in polar ice [10,14]. Accordingly, the studies of ice air trapped in ice cores show that CH_4 has sustained a stable atmospheric abundance for centuries prior to the industrial revolution. It was accepted that the background concentration of CH_4 was in the range of 1.4-1.6 ppm in the northern hemisphere and slightly less in the southern hemisphere [14]. For example, see Fig 2.2, based on their ice core data, find the methane concentration in the atmosphere was relatively constant at 0.7 ppm until about 150 years ago when it started to rise [15]. However, the concentration appears to have been increasing in recent years at a rate of 1-2 % per year [10, 14, 16].

[h]

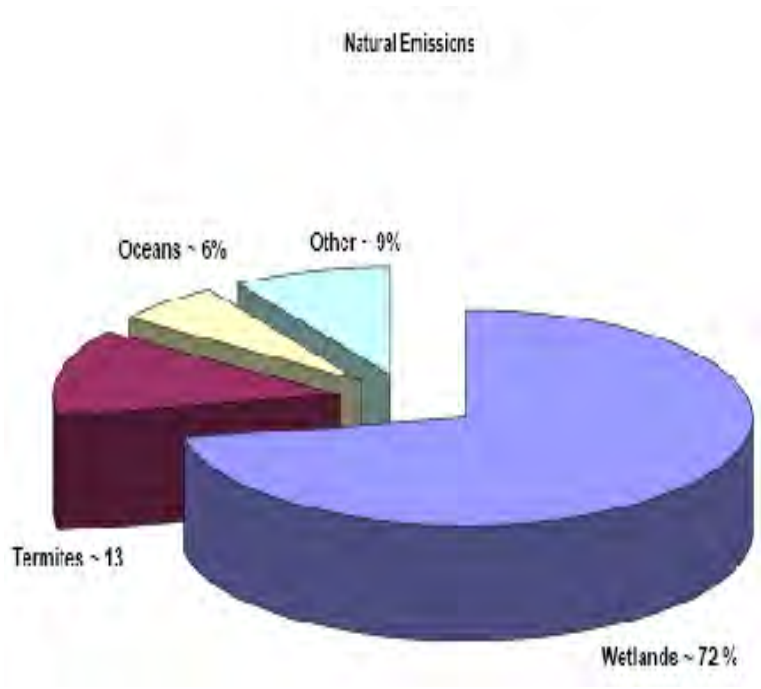

Figure 2.4: Natural emission

Due to its relatively short life time in the atmosphere (9-15 years) and its global warming potency, on a per molecule basis, it is more effective as a greenhouse gas than carbon dioxide. Methane has a direct effect on the radiative balance of the troposphere because of its strong IR absorption at 7.66 μm where CO_2 and H_2O absorb only weakly [17]. At 1750 ppbv, its current globally averaged tropospheric mixing ratio is more than twice as high as in preindustrial times [9].

Methane is also the most abundant reactive trace gas in the troposphere and its reactivity is important to both tropospheric and stratospheric chemistry. The oxidation of CH_4 by hydroxyl OH in the troposphere leads to the formation of formaldehyde CH_2O, carbon monoxide CO, and, with sufficient nitrogen oxides NO_x, to ozone O_3. Along with CO, methane helps control the amount of OH in the troposphere. Methane also affects the concentrations of water vapor and ozone in the stratosphere and plays a key role in the conversion of reactive chlorine to less reactive HCl in the stratosphere.

Once emitted, methane is removed from the atmosphere by a variety of processes, frequently called sinks. The balance between methane emissions and methane removal processes ultimately determines atmospheric methane concentrations, and how long methane emissions remain in the atmosphere. The dominant sink is oxidation by chemical reaction with hydroxyl radicals OH.

The increasing rate of methane emission may have significant impact on future global warming which has become a serious concern. This concern has stimulated the efforts

to quantify the potential of ecosystem as sources of atmospheric methane to develop policies and plans for controlling methane emissions, like Kyoto Protocol.

2.2 Methane chemistry and troposphere

Methane oxidation in the natural troposphere occur by the attack of the hydroxyl radical extracting hydrogen from CH_4 forming water in NO reach environment [12]:

$$CH_4 + OH \rightarrow CH_3 + H_2O \tag{2.2.1}$$

$$CH_3 + O_2 + M \rightarrow CH_3O_2 + M \tag{2.2.2}$$

The methyl radical, CH_3, formed at the same time reacts with oxygen forming a methylperoxy radical, CH_3O_2. In a continental atmosphere during the day, this will probably react with nitric oxide, NO, released by combustion processes, to form a methoxy radical, that in turn reacts with oxygen to form formaldehyde, $HCHO$:

$$CH_3O_2 + NO \rightarrow CH_3O + NO_2 \tag{2.2.3}$$

$$CH_3O + O_2 \rightarrow HCHO + HO_2 \tag{2.2.4}$$

Like methane, the formaldehyde molecule itself may be oxidized by OH in a similar sequence of reactions, the end result being the formation of CO or $CO2$ and water. The hydroperoxy radical, HO_2, from reaction Eq (2.2.4) oxidizes NO to NO_2 and regenerates an OH radical:

$$HO_2 + NO \rightarrow OH + NO_2 \tag{2.2.5}$$

The reaction sequence, Eq (2.2.1) to Eq (2.2.5), constitutes a chemical chain reaction with OH as the chain carrier: OH is consumed in reaction Eq (2.2.1) and regenerated

in reaction Eq (2.2.5). The OH radical can thus be regarded as a catalyst, only a small amount being needed to oxidize much larger amounts of CH_4. In the same reaction chain, two molecules of NO are also oxidized to nitrogen dioxide, reactions Eq (2.2.3) and Eq (2.2.5) [13]. NO_2 is short lived day time forming NO by photolysis:

$$NO_2 + h\nu(\lambda < 400nm) \rightarrow NO + O \tag{2.2.6}$$

$$O + O_2 + M \rightarrow O_3 + M \tag{2.2.7}$$

net

$$CH_4 + 8O_2 + 5h\nu \rightarrow CO + 4O_3 + 2OH + H_2O \tag{2.2.8}$$

Through the formation of formaldehyde $HCHO$ and its subsequent photo dissociation, for each molecule of methane four molecules of ozone are formed and two hydroxyl radicals, while carbon is oxidized to carbon monoxide. CO may react, as we have seen already, with H_2O but the result of this new oxidation cycle depends critically on the content of nitrogen oxide. In NO poor environments, CH_4 is oxidized to CH_2O by either of the following two pathways:

$$CH_4 + OH \rightarrow CH_3 + H_2O$$

$$CH_3 + O_2 + M \rightarrow CH_3O_2 + M$$

$$CH_3O_2 + HO_2 \rightarrow CH_3O_2H + O_2 \tag{2.2.9}$$

$$CH_3O_2H + h\nu \rightarrow CH_3O + OH(\lambda < 330nm)$$

$$CH_3O + O_2 \rightarrow CH_2O + HO_2 \tag{2.2.10}$$

net

$$CH_4 + O_2 \rightarrow CH_2O + H_2O$$

or

$$CH_4 + OH \rightarrow CH_3 + H_2O$$

$$CH_3 + O_2 + M \rightarrow CH_3O_2 + M$$

$$CH_3O_2 + HO_2 \rightarrow CH_3O_2H + O_2 \tag{2.2.11}$$

$$CH_3O_2H + OH \rightarrow CH_2O + H_2O + OH$$

net

$$CH_4 + OH \rightarrow CH_2O + 2H_2O \tag{2.2.12}$$

Here it is, however clear that hydroxyl and perhydroxyl radicals are being lost

Three reaction pathways lead to the further oxidation of formaldehyde to carbon monoxide

$$CH_2O + h\nu \rightarrow H + CHO(\lambda \leq 350nm) \tag{2.2.13}$$

$$CHO + O_2 \rightarrow CO + HO_2 \tag{2.2.14}$$

net

$$CH_2O + 2O_2 \rightarrow CO + 2H_2O$$

2.3 Methane chemistry and stratosphere

Although about 85 % of the total emissions of methane is consumed by reaction with tropospheric hydroxyl [18], the remaining methane flux, on average about 60 teragrams of methane per year (Tg CH4 / year), enters the stratosphere. In the stratosphere and above, the reaction with OH continues to be the dominant sink, but reactions with chlorine atoms and excited oxygen atoms are also important.

The most important chlorofluromethane, $CFCl_3$ and CF_2Cl_2 absorb uv radiations in the 190-220nm range, which results in the photo dissociation reaction [11]

$$CFCl_3 + h\nu \rightarrow CFCl_2 + Cl \tag{2.3.1}$$

$$CF_2Cl_2 + h\nu \rightarrow CF_2Cl + Cl \tag{2.3.2}$$

The free chlorine atom can react with methane to give hydrogen chlorine:

$$Cl + CH_4 \rightarrow HCl + CH_3 \tag{2.3.3}$$

$$Cl + H_2 \rightarrow HCl + H \tag{2.3.4}$$

The presence of the above reaction in both layers of the atmosphere tells us that the concentration of methane is declining with altitude. In the next chapter we will see the field atmosphere interaction type and radiative transfer theory that will help us determine the VMR of Methane consequently see the aforementioned property.

Chapter 3

Electromagnetic wave interaction mechanisms in the Earth's atmosphere

The interaction of electromagnetic waves with in Earth's atmosphere involves resonant interactions corresponding to molecular and atomic levels, non resonant interactions, and refraction [1]. But for the sake of our interest only resonant interaction is discussed below.

3.1 Resonant interaction

When electromagnetic wave interact with gaseous molecule, it may excite the molecule to higher energy level and in the process transfer all or part of energy to the molecule [1]. A molecule in an excited state may drop to a state with a lower energy level and in the process emit energy in the form of an electromagnetic wave. The energy levels of gaseous molecules are well defined and discrete. Thus, the related interaction occurs at a very specific frequency lead to spectral lines. The environmental factors, specifically, temperature and pressure lead to broadening of these lines to narrow bands.

The mid-infrared absorption spectra of molecules in the atmosphere are a result of simultaneous rotational and vibrational energy level transitions of these same molecules. Such spectra present themselves as bands of absorption with fine structure, where the central wave number of the band is determined by the type of vibrational transition taking place (fundamental, first overtone, etc.) while the band structure itself is determined by the allowed rotational transitions for that particular vibrational transition; the energy required to effect a rotational transition is much smaller than that required to effect a vibrational transition. The basic mechanisms behind the energy states of gaseous molecules and the shapes of spectral lines are briefly discussed here.

3.2 Rotational transitions

Pure rotational transitions are observed for molecules with permanent electric dipole moments e.g. HCl, CO, OCS that can interact with the incident electromagnetic radiation. This excludes homonuclear diatomic molecules (e.g. O_2 and N_2, except where a collision-induced dipole moment is present), linear molecules with a center of symmetry (e.g. CO_2, C_2H_2) and spherical top molecules (e.g. CH_4). The selection rules for rotational transitions of linear molecules are $\triangle J = \pm 1$ ($\triangle$ J is the change in the rotational quantum number) and typical energy separations between rotational levels are 10 cm^{-1} or less. This energy spacing is reduced by deviations of a molecule from the rigid rotor approximation (at high J values) and by heavy isotope substitution. Finally, the intensity of an observed transition is proportional to the transition

probability, the population and degeneracy of the initial energy state and the path length of the sample.

3.3 Vibrational transitions

A molecule with N atoms has 3N degrees of freedom for its motion. Since two sets of three degrees of freedom are required to describe the translational and rotational motion of the center of mass of the molecule, this leaves 3N-6 degrees of freedom for vibration in the molecule (3N-5 for linear molecules since only two degrees of freedom are necessary to describe the rotational motion of the center of mass). To a first approximation, a vibrating diatomic molecule can be described as a Simple Harmonic Oscillator (SHO) with the vibrational selection rule of $\triangle\nu = \pm 1$, $\triangle\nu$ is the change in the vibrational quantum number) and a typical spacing between vibrational levels of 1000 cm^{-1} [5]. Since the bonds of real molecules do not obey Hookes law (due to, e.g. nonlinear dipole moment variation with atomic displacement) the SHO transforms into an Anharmonic Oscillator with different vibrational selection rules ($\triangle\nu = \pm 1, \pm 2, \pm 3, \ . \ . \ .$). Transitions from energy levels other than the ground state are known as hot bands because they only become significant at high temperatures when the populations of higher energy levels increase; therefore, only the ($\triangle\nu = \pm 1, \pm 2, \pm 3, ...$) (from the ground state) are of practical importance. As a further consequence of anharmonicity, the spacing between each vibrational energy level decreases with increasing vibrational energy.

Finally, in addition to the fundamental modes and their weaker overtones, combination and difference bands are also permitted e.g. $\nu_1 + \nu_2$ or $2\nu_1 - \nu_2$, however, their

intensities are generally very weak. The weak combination/difference or overtone bands can sometimes be greatly enhanced at the expense of a nearby (accidentally degenerate) fundamental band in a process referred to as Fermi resonance. In addition to changes in intensity, the frequency of the higher (lower) band can also be further raised (lowered).

3.4 Rotational-vibrational transitions

Under the Born-Oppenheimer approximation, a diatomic molecule undergoes vibrational and rotational transitions independently of one another, since the energy scales are separated by two to three orders of magnitude. (We neglect electronic transitions in this discussion, whose energy scales are another two to three orders of magnitude higher than vibrational energy scales.) The selection rules for simultaneous but independent rotational and vibrational transitions can be shown to be a combination of the selection rules for each transition [19]

$$\triangle\nu = \pm, \pm 2, \pm 3, ... \tag{3.4.1}$$

where, $\triangle J = \pm 1$.

Strictly speaking, $\triangle\nu = 0$ is allowed and corresponds to a purely rotational transition, however $\triangle$J = 0 is, in general, not allowed for a diatomic molecule, i.e. a vibrational transition must, in general, be accompanied by a rotational transition.

The discussion of rotational-vibrational spectra up to this point applies only to diatomic molecules, which are by definition linear. It turns out that the rotational transitions of complex molecules also depend on the vibrational transition that the molecule is undergoing. For a linear polyatomic molecule (e.g. CO_2) if the vibration

is causing a dipole moment change that is parallel to the principal axis of rotational symmetry then the selection rules remain the same (although the spectra may still become unresolved for heavy molecules where the rotational line spacing becomes very small). On the other hand, if the dipole moment change caused by the vibration has a component that is perpendicular to the principal axis of rotational symmetry then $\triangle$J = 0 ceases to be forbidden and a vibrational transition becomes possible without a rotational transition. Since such vibrational transitions can and do occur at all rotational levels, an intense Q-branch appears in the spectrum at the band center, between the P and R branches. Finally, the spectra of molecules with more complicated geometries (symmetric tops (e.g. CH_3Cl), asymmetric tops (e.g. O_3, H_2O), spherical tops (e.g. CH_4) are increasingly complex, and require the introduction of a supplementary rotational quantum number K.

3.5 Spectral line Shape

Three fundamental processes interact to determine the observed shape of spectral lines. These are the natural line width, pressure broadening, and Doppler broadening. Natural line width, which arises from the Heisenberg uncertainty principle, is unimportant in planetary atmospheres. Pressure- and Doppler-broadening effects dominated line shapes in planetary atmosphere. However, the processes determining natural line widths and pressure broadening of lines are statistically identical, so these two processes have the same analytical form. In planetary atmospheres, Doppler broadening is intermediate in importance between natural line shape and pressure broadening or collision broadening. At pressures weaker than about 1 mb collisions become infrequent enough that the line shapes transition from Lorentzian

to Doppler. In this transitional regime the line shape is a convolution of Lorentzian and Doppler shapes.

3.5.1 Line Shape Factor

The fundamental property of a discrete line transition is the spectral absorption cross section, $\kappa(\nu)$, which measures the strength of the transition as a function of frequency (or wavelength, etc.) The absorption coefficient $k(\nu)[1/cm^{-1}]$ that describes a broadened transition line is modelled as the product of the line strength with the broadening function f$(\nu - \nu_o)$

$$k(\nu) = S(\nu_o, T) f(\nu - \nu_o) \tag{3.5.1}$$

where $f(\nu - \nu_o)$ satisfy

$$\int_0^\infty f(\nu - \nu_o) d\nu = 1 \tag{3.5.2}$$

The integrated absorption cross-section gives line strength or line intensity:

$$S = \int_0^\infty k(\nu)(\nu) d\nu \tag{3.5.3}$$

The line strength at two different temperature and frequency are related by

$$S(\nu, T) = S(\nu_o, T_o) \frac{Q(T_o \exp(\frac{-E''}{kT}))(1 - \exp(\frac{hc\nu_o}{kT})}{Q(T) \exp(\frac{-E''}{kT_o}))(1 - \exp(\frac{-hc\nu_o}{kT_o}))} \tag{3.5.4}$$

where T_o is a referense temperature of 296 K, Q is the partition function, E'' is the lower state energy of the transition, h is the Planck constant, c is the speed of light, and k is the Boltzman constant.

3.5.2 Pressure broadening

Collisions between molecules are the most important cause of line broadening in the lower atmosphere. Statistically, collisions in a gas of molecules of uniform speeds take place at random time intervals about a mean value. As with spontaneous decay, the probability distribution of time intervals between collisions is therefore a gaussian distribution. In reality, molecular velocities are not uniform but obey the Maxwell distribution.

$$p_M(v)dv = (\frac{M}{2\pi kT})^{\frac{1}{2}} exp(\frac{-Mv^2}{2kT})dv \tag{3.5.5}$$

where $p_M(v)$ is the probability that a molecule of mass M at temperature T has a velocity in [v; v+dv]. Collision-induced line broadening, or pressure broadening of lines is governed by a Lorentz line shape [3]

$$f_(\nu - \nu_o)(\nu, p, T) = \frac{\alpha_p}{\pi(\nu - \nu_o)^2 + \alpha_p^2} \tag{3.5.6}$$

where the half width at half-maximum intensity due to pressure (collision) broadening, α_p is called the pressure-broadened line width. Because α_p characterizes collisional interactions, its value depends on the concentrations and masses of all the molecular species which are present. Thus its determination is somewhat involved. The absorption cross-section for Lorentzian lines may now be written:

$$\alpha(\nu) = S\frac{\alpha_p}{\pi(\nu + \nu_o)^2 + \alpha_p^2} \tag{3.5.7}$$

From the kinetic theory of the gases the dependence of the half width α on the pressure and temperature is given

$$\alpha_p = \alpha_o(\frac{p}{p_o})(\frac{T_o}{T})^{\frac{1}{2}} \tag{3.5.8}$$

where α_o is the width at the standard pressure p_o and temperature T_o [3]. The actual Lorentzian half width α_p is calculated for the actual temperature T and actual pressure p from the related reference Lorentzian half width α_o measured at reference pressure p_o and reference temperature T_o.

3.5.3 Doppler broadening

Brownian motion causes molecules to constantly change their relative motion to the photons which may interact with them. While the frequencies of resonant absorption are constant in the frame of motion of the molecule, this random motion broadens the range of resonant frequencies in the frame of a stationary observer. This form of line broadening is called Doppler broadening. The probability that the molecule and a stationary reference frame (an observer) have relative velocity in [v; v + dv] is given by the Maxwell distribution.

$$p_M[\nu(v)]d\nu = (\frac{M}{2\pi kT})^{\frac{1}{2}} \exp(\frac{Mc^2\triangle\nu^2}{2\nu_o^2 kT})\frac{dv}{d\nu}d\nu$$

$$= \frac{c}{\nu_o}(\frac{M}{2\pi kT})^{\frac{1}{2}} \exp[-\triangle\nu^2\frac{2(\nu_o)^2 kT}{M^2 c}]d\nu \tag{3.5.9}$$

The Doppler line shape f_D and width α_D are defined as follows

$$f_D(\nu, T) = \frac{1}{\alpha_D}(\frac{\ln 2}{\pi})^{\frac{1}{2}} \exp[-\ln 2(\frac{\nu - \nu_o}{\alpha_D})^2] \tag{3.5.10}$$

$$\alpha_D(T) = \frac{\nu_o}{c}\sqrt{\frac{2kT}{M}\ln 2} \tag{3.5.11}$$

It is clear to recognize from Eq (3.5.11) that the Doppler broadened line have a shape of a form of Gaussian distribution.

3.5.4 Voigt Line Shape

In the atmosphere above 40 km where gases are at low pressure, it becomes important to incorporate the combined influence of the Lorentz and the Doppler in the infrared transfer calculations [3]. If we assume these two processes are independent but occur simultaneously, then the net line shape of the total process will be the collision-broadened line shape, shifted by the Doppler shift and averaged over the Maxwell distribution. The resulting line shape is called the Voigt profile, $f_\nu(\nu)$ [10]. The line parameters and absorption cross section in the above equation are compiled in the HITRAN software.

$$f_{(\nu-\nu_o)}(v,p,T) = \frac{1}{\alpha_D}\sqrt{\frac{\ln 2}{\pi}}\frac{y}{\pi}\int_{-\infty}^{\infty}\frac{\exp -t^2}{[(\alpha-t)^2+y^2]}dt \tag{3.5.12}$$

where y $= \frac{\alpha_p}{\alpha_D}\sqrt{\ln 2}$, t $= (\frac{\nu-\nu_o}{\alpha_D})\sqrt{\ln 2}$ and, α_p and α_D are Doppler and Lorentzian half widths, respectively and ν_0 is the central wave number that are directly adopted from the Hitran database

3.5.5 HITRAN spectral database

HITRAN (High Resolution Transmission)database is an acronym for high-resolution transmission molecular absorption database. HITRAN is a compilation of spectroscopic parameters that a variety of computer codes use to predict and simulate the transmission and emission of light in the atmosphere. It is an international standard compilation of absorption parameters that enables the calculation of atmospheric spectral simulations from the microwave through the visible. It contains reference temperature and pressure, line strength, line positions, transition intensities, air broadened and self broadened half width's (HWHM) and lower state energies ($E^{''}$), vibrational-rotational transitions of the 39 most atmospheric molecules. The

database is a long-running project started by the Air Force Cambridge Research Laboratories (AFCRL) in the late 1960's in response to the need for detailed knowledge of the infrared properties of the atmosphere [6].

3.6 Radiative transfer theory

Electromagnetic radiation can interact with matter through three basic mechanisms, absorption, scattering and emission [11]. A pencil of radiation occupying the solid angle $d\Omega$ is attenuated in proportion to the density and absorption characteristics of the medium through which it passes. Energy can be scattered out of the solid angle, which likewise attenuates energy following through $d\Omega$. Together absorption and scattering constitute the net extinction of energy passing through the pencil of radiation. Conversly energy emitted in to the solid angle or scattered in to $d\Omega$ from other direction intensifies the flow of energy through the pencil of radiation. These interactions are governed by a series of law that describe the transfer of radiation through matter, which is explained by radiative transfer theory. For retrieval of atmospheric state parameters from remote measurements the accurate modelling of atmospheric radiative transfer is basic component of retrieval theory [20].

3.6.1 Radiative transfer equation

Radiative transfer equations are the mathematical description for the process of transfer of electromagnetic-radiation through the gaseous atmosphere and its interaction with the atmosphere. The integro-differential equation describes the total change in the spectral intensity, or radiance as it traverses an infinitesimal distance through an optically active medium which can absorb, emit, and scatter electromagnetic energy

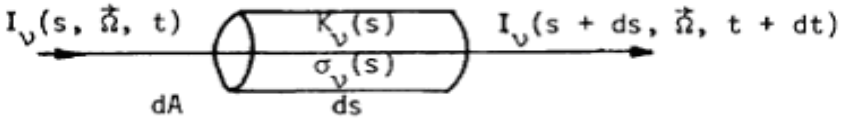

Figure 3.1: The change in intensity of a monochromatic beam of radiation as it passes through an optically active medium of length ds.

in the wavelength interval $d\nu$ centered about ν.

Consider a volume of gas in Fig 3.1 in which emission as well as absorption now takes place. The equation of energy transfer can be written, for monochromatic radiation or the radiant energy absorbed and scattered by the gas along the path is given by [12]:

$$dI_\nu(s,\Omega) = -k_\nu I_\nu(s,\Omega)ds - \sigma_\nu I_\nu(s,\Omega)ds \tag{3.6.1}$$

where ρ_a, is the density of the radiatively active gas (which is not generally the same as the total gas density ρ), k_ν and σ_ν are absorption and scattering coefficient respectively. If the gas is also emitting photons of frequency ν, then the total energy emitted by the volume element into the direction Ω is given by:

$$dI_\nu = j_\nu \rho_a ds \tag{3.6.2}$$

where j_λ is the source function coefficient. Including both emission and extinction we therefore obtain the radiative transfer equation(also called Schwarzschild's equation)[3] as

$$dI_{\nu(s,\Omega)} = j_\nu \rho_a ds - k_\nu \rho_a I_\nu ds - \sigma_\nu I_\nu \rho_a ds \tag{3.6.3}$$

Finally, we divide through $k_\nu(s) + \sigma_\nu(s)$ and write Eq (3.6.3) as

$$\frac{dI_{\nu(s,\Omega}}{(k_\nu(s)+\sigma_\nu(s))ds}+I_\nu(s,\Omega)=J_\nu(s,\Omega) \tag{3.6.4}$$

where

$$J_\nu(s,\Omega)=\frac{j_\nu}{k_\nu(s)+\sigma_\nu(s)} \tag{3.6.5}$$

is referred to as the source function. Defining the spectral volumetric extinction coefficient [21] as

$$\beta_\nu(s)=k_\nu(s)+\sigma_\nu(s) \tag{3.6.6}$$

and β_ν, ρ_a, and J_ν are given as functions of distance s, a formal solution of the radiative-transfer equation using optical thickness $\tau_\nu=\beta_\nu ds$ which the sum of both gases and aerosols as a variable [31] can be written as follows:

$$I_{(\nu,s)}=I_{(\nu,0)}\Gamma_\nu(s,0)+\int_s^{s'} J_\nu\frac{d}{ds'}\Gamma_\nu(s',s)ds' \tag{3.6.7}$$

where $I_{(\nu,0)}$ is the radiance at wave number ν incident at one end of the path, $I_{(\nu,s)}$ is the radiance emerging at the other, $\Gamma_\nu(s',s)$ is the transmittance of the path from s' to s, and J_ν depends on both thermal emission and scattering. In local thermodynamics equilibrium (LTE) it is given by:

$$J_{s'}=[1-\varpi(\nu)]B[\nu,T(s')]+\frac{\varpi(\nu)}{4\Pi}\int_{4\Pi} I(\nu,s,\Omega')P(\nu,\Omega,\Omega')d\Omega \tag{3.6.8}$$

where $B[\nu,T(z')]$, is the Planck function at temperature $T(z')$, $\varpi(\nu)$ is the single scattering albedo, the ratio of the scattering coefficient to the total extinction coefficient:

$$\varpi(\nu)=\frac{\sigma_\nu}{k_\nu+\sigma_\nu} \tag{3.6.9}$$

$I(\nu, s, \Omega^{'})$ is the radiance incident at s from direction, $\Omega^{'}$, and $P(\nu, \Omega, \Omega^{'})$ is the phase function from $\Omega^{'}$, into Ω.

Most instruments have a finite spectral bandpass, so that the quantity measured in channel l with normalized spectral response is $F_l(\nu)$ is:

$$I_l(z) = \int F_l(\nu) I_{(\nu,0,z)} d\nu + \int F_l(\nu) \int_0^z J[\nu, T(z^{'})] \frac{d\Gamma(\nu, z^{'}, z)}{dz^{'}} dz^{'} d\nu \qquad (3.6.10)$$

where $\int F_l(\nu) d\nu$=1.

From Eq (3.6.7), in the absence of emission ($J_\nu = 0$), the spectral radiance falls exponentially, decreasing by a factor of e over a distance corresponding to unit optical path. A region is said to be optically thick at a frequency ν if the total optical path τ_ν through the region is greater than 1 and optically thin if the total optical path is less than 1. A photon is likely to traverse an optically thin region without absorption or scattering [23].

The radiance I_ν reaching s thus has a simple interpretation [22], as follows. The first term on the right-hand side of Eq (3.6.7) represents the radiance at the starting point $s = 0$, attenuated by an exponential factor due to extinction over the distance s, while the integral represents the sum of contributions emitted from elements ds' at different distances s' along the path, each attenuated by the factor $\exp[-k_\nu \rho_a (s - s')]$ due to extinction over the remaining distance $s - s'$.

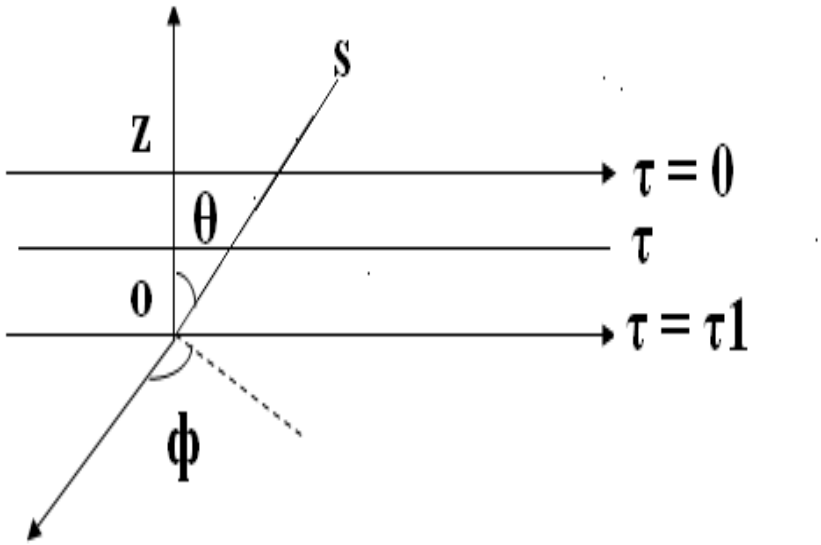

Figure 3.2: Geometry for plane-parallel atmosphere

3.6.2 Radiative transfer equation for plane parallel atmosphere

Consider a medium composed of planar layers perpendicular to axis oz, the electromagnetic property of the medium being constant in each medium. Let s be the length measured in the arbitrary direction Ω positive direction of axis OZ on Fig 3.2.

Taking μ as the cosine of angle θ between the radiation transmission direction Ω and axis OZ [12], i.e.,

$$\mu = \cos\theta \tag{3.6.11}$$

Then Eq (3.6.4) takes the following form [21]

$$\mu \frac{dI_\nu}{d\tau}(\tau, \mu, \varphi) = I_\nu(\tau, \mu, \varphi) - J_\nu(\tau, \mu, \varphi) \tag{3.6.12}$$

The general equation of transfer derived in Eq (3.6.12) may then be expressed for a

nonscattering atmosphere in the wave number domain as [3]

$$\mu \frac{dI_\nu(\tau_1;\mu)}{d\tau} = I_\nu(\tau,\mu) - B_\nu(T) \tag{3.6.13}$$

for upward intensity and

$$-\mu \frac{dI_\nu(\tau_1;-\mu)}{d\tau} = I_\nu(\tau,\mu) - B_\nu(T) \tag{3.6.14}$$

for downward intensity

Hence the solution for the upward and downward intensities are respectively given as:

$$I_\nu(\tau;\mu,\phi) = I_\nu(\tau_1;\mu,\phi)\exp(-\frac{(\tau_1-\tau)}{\mu}) + \int_\tau^{\tau_1} B_\nu[T(\tau')]\exp(-\frac{(\tau'-\tau)}{\mu})\frac{d\tau'}{\mu} \tag{3.6.15}$$

and

$$I_\nu(\tau;-\mu,\phi) = I_\nu(0;-\mu,\phi)\exp(-\frac{\tau}{\mu}) + \int_0^{\tau} B_\nu[T(\tau')]\exp(-\frac{(\tau-\tau')}{\mu})\frac{d\tau'}{\mu} \tag{3.6.16}$$

A quantity which plays an important role in the theory of infrared transfer in the atmosphere is the transmissivity Γ_ν, which is the ratio of transmitted to incident radiation, emission being neglected [22]. The absorption, as expressed by the transmittance function, may be due to molecular vibration-rotation transitions, Transmittance related to the absorption coefficient by:

$$\Gamma_\nu = \exp(-\int_0^z \kappa_p \rho dz) \tag{3.6.17}$$

where z is an arbitrary height. If we express this equation in pressure coordinates based on the hydrostatic equation and the definition of mixing ratio $q = -\frac{\rho}{\rho_a}$, where ρ and ρ_a are the density of gas and air respectively we obtain:

$$\rho dz = -\frac{q}{g}dp \tag{3.6.18}$$

and the monochromatic transmittance is given by:

$$\Gamma_(\nu, p_1, p_2) = \exp(-\frac{1}{g}\int_{p_1}^{p_2} k(\lambda, p^{'})q(p^{'})dp^{'}) \tag{3.6.19}$$

The spectral interval over which we wish to compute the transmissivity must in general contain many lines. It should be noted that there are many absorbers along the optical path so that the absorption cross section is weighted and given by [12]:

$$\kappa_\nu = \sum_{i=1}^{j} \kappa_i q_i \tag{3.6.20}$$

where q_i stands for volume mixing ratio VMR and absorption cross sections of the species i of the total number j of different molecular species that absorb in the spectral region under consideration. Hence Eq (3.6.20) becomes:

$$\Gamma_\nu = \exp(-\int_0^s \sum_{i=1}^{j} \kappa_{im} q_i \rho ds) \tag{3.6.21}$$

where, the strength k_{im} of the m^{th} line of the i^{th} absorber is temperature dependant, and is normalized shape $f_{im}(\nu, p(z^{''}), T(z^{''}))$ may also depend on pressure p. Furthermore, the absorption cross section of each species depends on the width of the absorption line which in turn highly influenced by pressure broadening effect at lower altitude and by Doppler at broadening effect at higher altitudes , while the line strength S also depends on the temperature. Due to the simultaneous occurrence of Lorentzian and Doppler broadening, voigt line profile is assumed for studies of infrared transfer in the earth's atmosphere. For the this line shape, the absorption coefficient of a line centered at ν_o is:

$$k(\nu) = \frac{y}{\gamma_D \pi^{\frac{3}{2}}} \int_{-\infty}^{\infty} \frac{\exp(-s^2)}{(x - t + y^2)} \rho_a ds \tag{3.6.22}$$

where x = $\frac{(\nu-\nu_o)}{\gamma_D}$ and y = $\frac{\gamma_L}{\gamma_D}$

Thus, the spectral transmittance now be explicitly written as:

$$\Gamma_\nu = \exp(-\int_0^s \sum_{i,m=1}^{j,M} k_{i,m} f_{i,m}(\nu, p(z^{''})) \frac{y}{\gamma_D \pi^{\frac{3}{2}}} \int_{-\infty}^{\infty} \frac{\exp(-s^2)}{(x-t+y^2)} \rho ds \tag{3.6.23}$$

The accurate transmittance profiles are normally derived by means of line by line modelling calculations[23], which involve the direct integration of monochromatic transmittance over the wave number spectral interval, weighted by an appropriate response function if so desired.

We consider plane parallel atmosphere is a good approximation for real atmosphere. In the next chapter, we consider inverse theory for atmospheric applications. An effort will be made on to use RTE and inverse method to infer atmospheric parameters from measured spectra.

Chapter 4

Inversion methods and retrieval theory

Inverse theory refers to the mathematical framework used in the inversion of complicated functions. In remote sounding of the atmosphere, the indirect quantities measured (e.g. radiances) must be inverted in order to derive the quantities that are desired (e.g. vertical trace gas or temperature or pressure distributions). The inverse problem is concerned with determining the state of the atmosphere, in particular the vertical distribution of the target molecules, from the observed absorption spectra. The process of deducing constituent distributions from observations of the Earths atmosphere is termed retrieval [24]. The quantities to be determined in most inverse problems are continuous functions, while the measurements are always of discrete quantities. Thus most inverse problems are ill-posed [23]. The retrieved profiles and total column amounts of the target species are the ones that provide the best representation of the truth, given the measurement and the a priori information, and their respective uncertainties. The retrieval process in the process of extracting vertical information of atmospheric state parameters from sequential spectra measurements of different altitudes in the case of space born sensors. In the case of ground based

sensors, the the process involves the use of spectral radiances measured at a certain zenith angle. The general remote sensing equation can be written as [23].

$$y = F(x, b) + \varepsilon \tag{4.0.1}$$

where y is the measurement vector (here the measured infrared radiances) and F(x,b) is the forward model which contains the physics of the radiative transfer process. x is state vector that specifies the atmospheric state (here the CH_4 concentration to be inferred from the measurement), and b represent all other components of the forward model which are predetermined: (pressure, temperature, other constituent profiles, surface emissivity, instrument spectral function, an spectroscopic parameters, surface height, geometry and trajectory of the spacecraft, etc. is the measurement error that is due to instrumental noise. The inverse problem is to determine x for a given y.

4.1 Forward Model

As given in Eq (4.0.1), the forward model relates the true atmosphere to the measured spectrum. Atmospheric spectra are simulated using a multi-layer, multi-species, line by line radiative transfer model originally developed at the NASA research Center for the solar spectra recorded with FTS. The model assumes the atmosphere is well represented as homogenous layer in local thermodynamic equilibrium and that the modelled spectra have a voigt profile, refractive ray tracing calculations are assumed to be separate and iterative [23]. The synthetic atmospheric spectra out put by the forward model are simulated based on a 41 layer atmosphere. Subsequent layers are defined with different kilo meter thickness up to 10 km, and with increasing thickness between 10 and 40 km. Between 40 and 80 km, layers have thick ness of 10 km and the upper boundary occurs at 100km.

4.2 Retrieval Method

Rearranging Eq (4.0.1) the least squares solution can be obtained by minimizing the cost function χ^2 after the equation has been normalized by the errors, where

$$\chi^2 = \varepsilon^T \varepsilon = (k \cdot x - y)^T (k \cdot x) \tag{4.2.1}$$

The gradient χ^2 leads to the normal equations:

$$k^T \cdot k \cdot x = k^T \cdot y \tag{4.2.2}$$

from which:

$$x = (k^T \cdot k)^{-1} k^T \cdot y \tag{4.2.3}$$

Eq (4.2.1) is true only for linear model, i.e for the case F(x,b) $\simeq$ kx, where k is the jacobian, but it is not true in our case. And it shows us that the inverse problem is undetermined problems where the number of independent equation is less than the number of unknowns. A fundamental obstacle in all inverse problems of remote sensing is the uniqueness of solution. The non-uniqueness arises because the medium under investigation may be composed of a number of unknown parameters whose various physical combinations may lead to the same radiation signature. There are also mathematical problems associated with the stability of solution.

The Optimal Estimation Method (OEM) is particularly well-suited to the under-determined problem of deriving a vertical profile of an atmospheric trace gas from a ground-based solar absorption spectrum. The problem is under-determined (ill-posed) in the trivial sense that we are seeking a continuous function from a finite set of measurements, however it remains under-determined even after we discretize the

desired vertical profile. This occurs because the spectral absorption features contain only enough information to distinguish a few independent vertical layers, however, the atmosphere must be forward modelled on 41 layers in order to avoid gross errors in the simulated spectra due to the misrepresentation of trace gas volume mixing ratio, temperature, and pressure. The vertical resolution of ground-based spectra is fundamentally limited by observation geometry, maximum achievable spectral resolution and measurement SNR.

In the OEM formulation of the ground-based remote sounding problem, a priori knowledge, x_a, of the n-dimensional state vector, x (vertical profile of the trace gas of interest) is combined with the m-dimensional measurement vector, y (high-resolution measurements of a spectral absorption feature) as a weighted mean.

It employs the Bayesian approach in solving the inverse problem. One requirement is that there are some prior understanding or expectation of the quantities we want to determine. We then want to determine this understanding based on new information [23].

As we have seen in the previous section, measurement process is expressed by a forward model which maps the state space (x) in to the measurement space (say y). Bayes theorem provides a formalism to invert this mapping and calculate a posteriori probability density function (PDF) by updating the aprior PDF with a measurement PDF.

Given the measurement error covariance matrix s_ϵ (this could be the noise in the spectra), the a priori x_a, and applying Bayes theorem, we arrive at a solution for $\hat{x}$, which is the most likely state i.e., the one for which P(x/y) is maximum, or the expected value solution [23]. According to Bayes expression:

$$P(x) = \int_{\infty}^{\infty} P(x, y)dy \tag{4.2.4}$$

where P(x) is the knowledge of x before the measurement is made and P(x,y) is the joint prior pdf of x and y. The two pdfs are given by

$$P(y) = \int_{\infty}^{\infty} P(x, y)dx \tag{4.2.5}$$

and

$$P(y/x) = \frac{P(x, y)}{\int_{\infty}^{\infty} P(x, y)dy} \tag{4.2.6}$$

Inserting Eq (4.2.5) into Eq (4.2.6) for the integral we obtain

$$P(y/x) = \frac{P(x, y)}{P(x)} \tag{4.2.7}$$

Then we obtain Baye's theorem as the relationship between the two different condition pdf's. When generalized for the vector case

$$P(x/y) = \frac{P(y/x)P(x)}{P(y)} \tag{4.2.8}$$

The left hand side of Eq (4.2.8), P(x/y), is the posterior pdf of the state when the measurement is given. This is what we want to update is the prior knowledge P(x) of the state with the measurement. P(y/x) describes the knowledge of y that would be obtained if the state were x. This method requires the minimization of a cost function which, for gaussian errors is

$$-2 \ln P(y/x) = (y - kx)^T s_\varepsilon^{-1}(y - kx) + c_1 \tag{4.2.9}$$

where c_1 is a constant and s_ϵ is the measurement error covariance, and

$$-2\ln P(x) = (x - x_a)^T s_a^{-1}(x - x_a) + c_2 \tag{4.2.10}$$

where x_a is the a priori value of x, and s_a is the associated covariance matrix

$$s_a = \varepsilon(x - x_a)(x - x_a)^T \tag{4.2.11}$$

Substituting Eq (4.2.9) and Eq (4.2.10) in Eq (4.2.8) we obtain for the posterior pdf:

$$-2\ln P(x/y) = (y - kx)^T s_\epsilon^{-1}(y - kx) + (x - x_a)^T s_a^{-1}(x - x_a) + c_3 \tag{4.2.12}$$

where P(y) which does not depend on x has been incorporated in to the c_3 along with the normalizing factors of P(y/x) and P(x). Eq (4.2.12) is quadratic in x, and hence it is possible to write it as

$$-2\ln P(x/y) = (x - \hat{x})^T \hat{s}^{-1}(x - \hat{x}) + c \tag{4.2.13}$$

By comparing the terms quadratic in x between Eq (4.2.12) and (4.2.13) Roders [23] shows that the covariance, $\hat{s}$, of the expected value, $\hat{x}$, is given by

$$\hat{s} = k^T s_\epsilon^{-1} k + s_a^{-1} \tag{4.2.14}$$

while the expected value itself is given by equating terms that are linear in x^T;

$$\hat{x} = (s_a^{-1} + k^T s_\epsilon^{-1})^{-1}(s_a^{-1} x_a + k^T s_\epsilon^{-1} y) \tag{4.2.15}$$

Hence the retrieved methane VMR ($\hat{x}$) is a weighted average of the a priori (climatological) value and the value derived solely from the measured radiances.

In deriving the optimal solution and its error covariance, we have assumed Gaussian error statistics and a linear or nearly linear forward model, allowing us to find the

optimal solution in one step. The inverse problem of deriving vertical profiles from infrared spectra is in fact moderately nonlinear, whereby the forward model linearalization is sufficient to carry out an error analysis and retrieval characterization in the vicinity of the optimal solution, however it is insufficient to find the optimal solution in one step in the first place. Grossly nonlinear problems are nonlinear even within the solution error bars, complicating matters even further. In the moderately nonlinear inverse problem, the weighting function matrix depends on the state, and hence, a solution must be found iteratively by evaluating k at each step of the iteration. We begin by taking the gradient of Eq (4.2.12);

$$\nabla_x[-2\ln P(x|y)] = -[\nabla_x F(x)]^T s_{\epsilon^{-1}}[y - F(x)] + s_a^{-1}[x - x_a] = 0 \tag{4.2.16}$$

Setting k(x) = $\nabla_x F(x)$ and for x = $\hat{x}$ at the minimum we can write

$$-[k(\hat{x})^T]s_\epsilon^{-1}[y - F(\hat{x}) + s_a^{-1}(x - x_a)] = 0 \tag{4.2.17}$$

which is an implicit equation for $\hat{x}$ that must be solved numerically. The right hand side of Eq (4.2.16) is the gradient of the cost function, g(x), which is again differentiated in the vector-equivalent of Newtons method

$$x_{i+1} = [\nabla_x g(x_i)]^{-1} g(x_i) \tag{4.2.18}$$

where the second derivative of the cost function $\nabla_x g$ follows from Eq (4.2.17):

$$\nabla_x g = s_a^{-1} + k^T s_\epsilon^{-1} k - [\nabla_x k^T][s_\epsilon^{-1}][y - F(x)] \tag{4.2.19}$$

When the third term of Eq (4.2.19) is small as is the case in what are known as small residual moderately nonlinear problems the Newton method becomes the Gauss-Newton method and yields the following iterative solutions for x_{i+1}:

$$x_{i+1} = x_i + (s_a^{-1} + k_i^T s_\epsilon^{-1} k_i)^{-1}[k_i^T s_\epsilon^{-1}(y - F(x)) - s_a^{-1}(x_i - x_a)] \tag{4.2.20}$$

where k_i is taken to mean k evaluated at x_i and y_i= $F(x_i)$.

By expressing x_{i+1} as a departure from x_a rather than x_i we can rearrange Eq (4.2.20) in both the n-form and the m-form, giving two other useful iterative solution:

$$x_{i+1} = x_a + (s_a^{-1} + k_i^T s_\epsilon^{-1} k_i)^{-1} k_i^T s_\epsilon^{-1}[y - F(x_i) + k_i(x_i - x_a)] \tag{4.2.21}$$

$$= x_a + s_a^{-1} k_i^T (k_i s_a k_i^T + s_\epsilon)^{-1}[y - F(x_i) + k_i(x_i - x_a)]$$

Neglecting the $\nabla_x k^T$ in Eq (4.2.19) is equivalent to assuming a Gaussian posterior PDF or linearity within the error bars of the iterated solution, i.e. that the problem is not grossly nonlinear. Finally, the covariance of the solution is evaluated as before, once $\hat{x}$ is found

$$\hat{s} = (\hat{k}^T s_\epsilon^{-1} \hat{k} + s_a^{-1})^{-1} \tag{4.2.22}$$

The averaging kernel matrix A relates the expected state to the true state through:

$$\hat{x} - x_a = G(y - kx_a) \tag{4.2.23}$$

where G is the gain matrix. It is trivial to show that the this matrix is represented as:

$$G = (s_a^{-1} + k^T s_\epsilon^{-1} k)^{-1} k^T s_\epsilon^{-1} \tag{4.2.24}$$

Therefore, the averaging kernels matrix is given by

$$A = Gk \tag{4.2.25}$$

and nothing that for a linear model $= A(x - x_a) + G\varepsilon$, Eq (4.2.23) can be written as

$$\hat{x} = Ax + (I - A)x_a + G\epsilon \tag{4.2.26}$$

where I is the identity matrix. It follows from Eq (4.2.26) that the retrieved profile is a smoothed version of the true profile. The retrieved value at a given level is an average of the true profile weighted by the corresponding averaging kernel(row of A) with additional error terms accounting for the a priori contribution and the spectral noise. The averaging kernel gives therefore the sensitivity of the retrieved value to the true profile. The position of its maximum indicates the altitude of maximum sensitivity, while its full width at half maximum (FWHM) is an estimation of the vertical resolution. According to Rodgers [23] the trace of the averaging kernel matrix gives the so-called degrees of freedom (DOF) for signal. This is an indication of the number of independent pieces of information contained in the measurement. A represents the averaging kernels of the state vector subspace containing the VMR profiles of a certain gas (in our case methane) in the atmosphere, that the DOFs represent approximately the number of independent layers that can be retrieved. For each 41 layers the full width at half maximum of the averaging kernels provides an estimate of the vertical resolution of the profile retrieved at the corresponding altitude, while the area of the averaging kernel represents the sensitivity of the retrieval at the corresponding altitude.

4.3 SFIT2

The SFIT2 code has its origin in SFIT1 [6] developed for ground-based retrievals of total column amounts. It is the extension of SFIT1 to retrieve trace gas profiles which was developed jointly by C. Rinsland of NASA Langley and B. Connor

of NIWA Lauder, NZ. The nonlinear least-squares algorithm was replaced with the optimal estimation algorithm used previously primarily for microwave remote sensing.

This incorporates a climatological covariance by specifying an assumed percentage variability of the a priori profile for each layer and a correlation length which is defined as an exponentially decaying intercorrelation between layers. The constraints imposed on the solution are weighted relative to the expected variance of the fit by specifying an assumed SNR value of the measurement, which is an input variable of SFIT2. The SFIT2 algorithm has been used in many previous analysis of ground-based high-resolution spectra.

Chapter 5

Retrieval inputs

The retrieval inputs used in this study are FTIR radiance data, methane a priori data, and ancillary data. The radiance data were taken by the FTIR campaign along Atlantic ocean covering our region of study. The measurements were taken in October and November 1996.

The problem of profile retrieval from remote sensing measurements is always underdetermined: a continuous profile of an atmospheric constituent is reconstructed from a finite number of measurements. The problems of this kind belong to the class of ill-posed problems. Measurement data themselves do not uniquely determine the solution; therefore, some kind of a priori constraint must be used to make the problem well-posed. Following [23], it can be done via prior information about atmosphere, which includes a mean state and its covariance. This prior state of methane, shown in Fig 5.1 that is used to constrain the retrieved state is taken from the climatological records. The validating data for the retrieved VMR for methane are obtained from HALOE satellite.

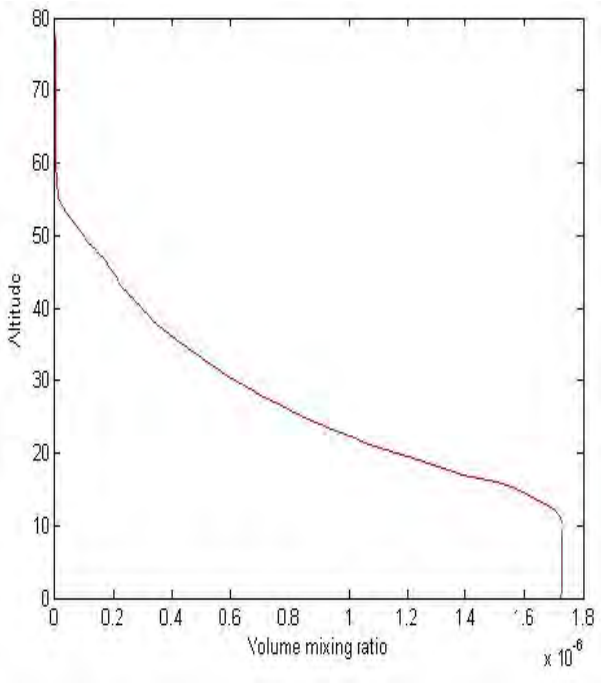

Figure 5.1: A prior VMR used for the retrieval of Methane

Selection of spectral microwindows

Deriving information about the vertical distribution of trace gases out of high resolution FTIR spectra is possible because of the line shapes. While the line center provides information about the higher altitudes of distribution, the wings of a line provide information about the lower altitudes. Therefore the information content of the retrieval will strongly depend on the choice of the absorption line. Microwindows are sets of consecutive grid points which are analyzed for retrieval of atmospheric state parameters rather than the spectrum as a whole. They are subsets of the complete FTIR spectra chosen to maximize the signal from the target species while minimizing the contributions from foreign species and other potential sources of error. The vertical spectral microvillous are selected such that they contains unsaturated

well-isolated absorption features of the target species with a minimal number of interfering molecular lines. It also focus at the amount on information present in the spectra, represented by the DOFS. Based on this methane is retrieved by using two microvillous that are 4265.3000 - 4265.7000 and 4277.6200 - 4277.9700 in which the interference of foreign gas is negligible as the absorption bands of these microwords is shown in Fig 5.3. These are directly adopted from Spectroscopic Atlas Atmospheric Microvillous in the Middle Infra-Red database [25]. In these microwords we identified eight interfering gases (CO, HI, OH, H_2O, HDO, NO, NH_3, N_2O) with the interference effect less than 1 %. Among all these gases only H_2O has 0.232 % and CO has 0.009 % contribution to the absorption in the related microwords with the intervention effect shown in the Fig 5.3, which are less than 1 to be neglected with out considering additional criteria.

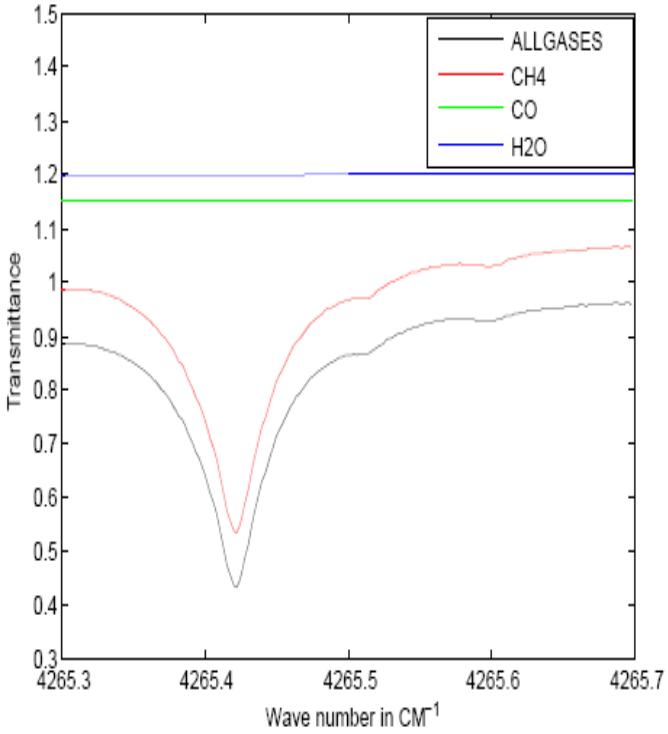

Figure 5.2: The absorption band in the micro-window range of (4265.3000 - 4265.7000)

Chapter 6

Historical understanding of atmospheric aerosols

6.1 What are aerosols?

Atmospheric aerosols usually means the mixture of solid and liquid particles, which referred to those solid and liquid particles suspended in the atmosphere [12]. Those atmospheric aerosols under above definition encompasses a broad array of different substances in troposphere, aerosols with widely varying sizes in micron and sub-micron ranges. Compared to atmospheric gases, aerosols are highly in homogeneous. This is due to widely varying aerosols microphysical properties, such as their sources, sinks and loading, composition, size distribution, chemical interaction, life time and diurnal variation, in space and time. Those and other properties of aerosols make their characterization on the global scale extremely difficult and observations have to be continuous. Atmospheric aerosols are originated from direct man's activities known as anthropogenic; examples of some of them are aerosols that originate from

biomass burning and industrial pollution. In other they originate from natural processes, such as, wind generated dust and sea spray, volcanic eruption, smokes from natural forest fire and so on. Also the natural production of aerosols by chemical reactions of precursor natural gases is the other organization of aerosols from natural processes, which are known as secondary particles.

Also the aerosol size distributions describe the number of aerosol particles observed in a certain radius size ranges, so based on it and aerosols size ranges categories we can study the origin of chemical interaction and other micro and macro physical properties of aerosols.

Aerosol particles range in size from 0.01 microns to several tens of microns. Cigarette smoke particles are in the middle of this size range; typical cloud drops are 10 or more microns in diameter. Under normal circumstances, the majority of aerosols reside in the troposphere (lower atmosphere), where they are washed out of the air in about a week by rain. Aerosols are also found in the stratosphere (the atmosphere just above the troposphere). A severe volcanic event, such as the Pinatubo eruption in the Philippines in 1991, can put large amounts of aerosol into the stratosphere. Since it does not rain in the stratosphere, these aerosols can last for many months, producing beautiful sunsets around the globe, and possibly causing summer temperatures to be cooler than normal.

With out defining it, early observation of atmospheric aerosols were carried out by visual observations. Aitken [27] designed an instrument to measure what we now

call Aitken particles (he called it dust). Mie [28] developed a theoretical approach for handling optically active particles today called Mie particles. Electrically charged atmospheric particles (charged ions) tended to be treated separately [29], as were radioactive particles [30]. Particles that deserve to nucleate cloud drops (cloud condensation nuclei) and ices in clouds (ice nuclei) also have been generally considered separately. Until recently, biological aerosols (other than pollen and spores) were almost neglected by the atmospheric aerosol community [31].

This type of departmentalization of atmospheric particles originated, in part, from the use of special measuring techniques. Even when Junge [32] published the first view of a continuous aerosols size distribution covering radii from 0.01 to 10 μm, the picture of different aerosol populations was still strong. Only subsequently did the view of a continuous atmospheric aerosol size distribution, with an analytical power function to describe it, shine through [34].

The concept of different aerosol populations also influenced research on the chemistry of atmospheric aerosols. Thus, there were publications on radioactive particles, Sulfate, nitrate [35], sea salt [36], organic particles and pollen [37], to name a few. This occurred despite the fact that the concept of 'mixed nuclei' (i.e., different compounds mixed together to form a single particles had long been understood) [38].

The subdivision of aerosols into different population might also reflect a desire to classify things to better understand them. Thus after Junge introduced the continuous

atmospheric aerosol size distribution he also classified them geographically into maritime, continental and background aerosols [39] and by size into Aitken (0.001-0.10 μm radius), large (0.1-1 μm), and giant (>1 μm) particles. It was pointed out that the plots together with the use of an analytical power function blurred the distinctive pattern of atmospheric aerosol modes. He introduced the terms nucleation mode (0.001-0.1μm), accumulation mode (0.1-1 μm), and coarse particle mode (1μ m). The nucleation mode was produced by gas-to-particle conversion (GPC), the accumulation mode by coagulation and heterogeneous condensation, and the coarse mode by mechanical process. While this process might act rapidly enough in regions of very high aerosol concentration typical of urban areas, they may not be as important for the troposphere aerosols in general (e.g., sea salt aerosol; [39], mineral aerosols; [39]).

6.2 Aerosol emission

Emission is a source of primary particles in the atmosphere. As stated above, in general aerosols are introduced into the atmosphere in to two ways; by emission and homogenous nucleation. Horizontal advection and vertical convection/eddy diffusion, and sedimentation also move particles in to or out of a region. Globally particle emission rates from natural sources exceed those from anthropogenic sources. In urban areas, the reverse is true. Nucleation may occur on the surface of an existing particle (heterogeneous nucleation) or in the absence of pre-existing surfaces (homogenous nucleation). Nucleation may also involve the agglomeration of one, two, or more types of molecules. The Following sub sections will present several types of natural and anthropogenic particle emission sources.

6.2.1 Aerosols of Marine origin

The ocean represent the largest natural aerosol of world-wide extent. The parent, material of the aerosol produced by them consists of sea salts, Primarily $NaCl$ [40]. The aerosol are formed from spray penetrating the atmosphere; fine air bubbles expelled from the surface of the water separate the surface and thus produce small droplets that decrease further in size in air by evaporation. Fig 6.1 shows the process of droplet formation in a schematic diagram. The rising air bubbles burst on the surface of the water. This results in a fine ascending jet of water that soon disintegrates into a number of approximately equal droplets (W), which may be transported to an altitude up to about 15 cm depending on their size. Their size amounts to about 1/10 of the bubble dimension. At the same time, a large number of much smaller water particles (M) can be observed in every such process; evidently these form during disintegration of the thin water film on the bubble surface. Both groups of droplets are exposed to air motion and ex-change, and are dispersed horizontally and vertically. In this process their size decreases by evaporation until they reach an equilibrium determined by the reactive humidity, salt concentration and the radius of concentrated salt solutions and beyond this, crystallization of the salt.

A further possibility for the entry of sea salt into the air consists of the removal of particles from wave crests by wind. The particles formed usually are considerably larger than those discussed above and have only a short life time, since they are rapidly deposited again. They are probably responsible for the occasionally very high salt concentration of 50-1000 $\frac{\mu}{m^3}$ of the air in the immediate vicinity of the coast extending only a few kilometers into the continent. Marine aerosols in the range of

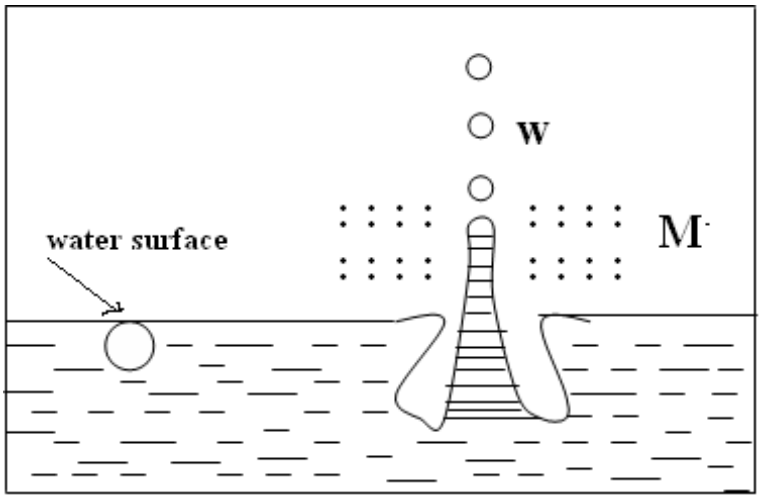

Figure 6.1: Formation of spray droplets during explosion of air bubbles from the surface of water(from trace element),W = droplets, M = Water particles

larger particles exhibit the same power distribution as a continental aerosols.

6.2.2 Soil-and Fugitive-dust emission

A major emission source of aerosol particles in the atmosphere is the lifting of soil dust and road dust by wind [12]. The wind picks up particles from the land surface particularly when the soil is dry and without plant cover and carries them great distances away from their source regions. These mineral aerosols are made up of materials derived from the Earth's crust and are therefore rich in iron and aluminium oxides and calcium carbonate. Most of the mineral aerosols in the air come originally from the desert regions, about half of the total mineral aerosols in the air come originally from the Saharan Desert(Fig 6.2). Primary aerosols emitted into the air as a result of mechanical processes such as wind erosion of soils to produce mineral aerosols or wave breaking to produce sea salt aerosol are large and known as coarse mode aerosols. These aerosols can have diameters of 10 m or more. Source regions

Figure 6.2: A river of Saharan dust flows over the Mediterranean sea and Italy on July 16, 2003. Source: NASA/Seawifs

of dust on a global scale include deserts (e.g., the Sahara in North Africa, Gobi in Mongolia and northern China, Mojave in southeastern California) and regions where foliage has been cleared by biomass burning and plowing. Deserts are continuously expanding due to land clearing and erosion on desert borders. Up to half of all wind-driven soil-dust emission worldwide may be anthropogenic.

6.2.3 Volcanic Eruptions

Volcanic eruptions inject enormous quantities of gases and aerosols in the atmosphere. Unlike the other sources of aerosols, the plume of ash coming from the volcano can be so high that the particles and gases can penetrate the stratosphere. The Pinatubo volcanic plume reached 40km in height [41]. Water vapor is the most abundant gas in magma, making up 50 to 80% of gas mass. Other important gases include carbon

Figure 6.3: St Helens erupting on May 18, 1980. Source: NASA

dioxide, sulfur dioxide, hydrogen sulfide(H_2S), Carbonyl sulfide (OCS), and molecular nitrogen. Minor gases include carbon monoxide, molecular hydrogen, molecular sulfur, hydrochloric acid, molecular chlorine, and molecular fluorine.

Particles that enter the upper atmosphere are not easily removed from the air back to the ground and volcanic material remains at the level injected for a long time (sometimes several years). The gases emitted by volcanoes also produce aerosols. Volcanos also emit particles that contain the elements of the Earth's Mantle. The most abundantly emitted particle components are silicate minerals(minerals containing Si). Other components include aluminium, iron, sulfate, nitrate, chloride, sodium, calcium, magnesium, potassium, black carbon, and organic matter. The emission rate of sulfate particles is only about 3% particles that of sulfur dioxide [48].

Volcanic gases, such as carbonyl sulfide and sulfur dioxide are sources of new particles. When OCS is injected volcanically into the stratosphere, some of it photolyzes. The product react to form sulfur dioxide gas, which oxidizes to form sulfuric acid gas, which homogenously nucleates to form new sulfuric acid-water aerosol particle, called the Junge layer, has formed in the stratosphere by this mechanism.

6.2.4 Biogenic aerosols

Particles which are produced by living organisms are called biogenic aerosols. Primary aerosols can be pollens, fungi spores, bacteria and viruses. Forest fires are another source of biogenic aerosols.

6.2.5 Anthropogenic aerosols

Particles emitted during human activity are called anthropogenic aerosols. Anthropogenic aerosols can be either large (coarse particles) or small (fine particles). Dust from roads and construction sites (such as cement works) produces coarse mode anthropogenic aerosols whereas small fine mode aerosols are generated from fossil fuel combustion in power generation and vehicles and from high temperature industrial processes such as metal smelting.

6.2.6 Biomass burning

Biomass burning aerosol consists of two major chemical components: black carbon (BC), which primarily absorbs solar radiation, and organic carbon (OC), which primarily scatters solar radiation. Sources of biomass burning aerosol include burning of forests and savanna for colonization and agriculture, burning of agricultural waste,

Figure 6.4: Sources of Anthropogenic aerosols

and substances burned for fuel such as wood, dung and peat. Not all biomass aerosol comes from anthropogenic activities, as naturally occurring vegetation fires regularly occur. The fraction of anthropogenic biomass aerosol remains difficult to deduce.

6.2.7 Secondary aerosols

Particles in the air can also result from gas-to-particle-conversion reactions. In this type of reaction new particles can form when molecules gather together in the air to form a species large enough to be considered a particle - this process is known as nucleation. Gases can also condense on pre-existing particles to form bigger aerosols.

Aerosols produced from gas-to-particle conversion reactions are small(less than 1 μm in diameter) and are known as fine mode aerosols. Most of the naturally formed secondary aerosols in the atmosphere are the result of sulphur gas emissions. In the

marine environment most sulphur is emitted as dimethyl sulphide (DMS) by phytoplankton. Reaction of DMS in the atmosphere forms sulphur dioxide (SO_2). On land decaying vegetation and animal material produces hydrogen sulphide (H_2S).

Natural sources produce also carbon containing gases which go onto form aerosols. Plants also emit biogenic gases which we call Volatile Organic Compounds. These biogenic gases can under go gas-to-particle-conversion reactions to form secondary aerosols. The annual emission of SO_2 from human activity has increased from 10 millions tons per year in 1860 to 150 millions tons per year in the 1980's. Anthropogenic emissions of sulphur containing gases now exceed natural emissions even though atmospheric SO_2 levels are now falling because of international legislation.

Humans also produce more and more nitrogen containing species that give rise to nitrate aerosols. The reaction of some anthropogenic compounds, emitted during combustion of petrol and during biomass burning, results in carbon containing aerosols.

Since early last decades, human being become highly curious about his environment and several satellite system have been lunched with missions to minor constituents. The first successful satellite experiment specially designed to monitor stratospheric aerosols on a continuous basis is the Stratospheric Aerosol Measurement II (SAM II). The Nimbus-7 satellite, which carries SAM II was launched October 1978, and continues to provide high latitude stratospheric aerosol data. The subsequent mission designed for aerosol measurements, the stratospheric Aerosol and Gas Experiment I (SAGE I), is aboard the application Explorer Mission returned 34 months of data

before operations were terminated [43]. Sage II, the third mission specially designed to monitor stratospheric aerosols, was launched from a space shuttle on 5 October 1984. A detailed description of SAGE II will be present in chapter 7. In addition a number of ground based instruments focusing on the same issue are emerging. Mobile Lidar system which is found in NLC-CSIR, Pretoria, South Africa is the prominent in African continent, which is one of the two Lidar system in Africa that are located only in South Africa. So to be sure of the information obtained from this lidar system it has to be validated by using the information from the space based instruments such as SAGE-II. Thus the validation will be performed by using the aerosol climatology from the SAGE-II satellite and will be presented in chapter 8.

Chapter 7

Stratospheric Aerosol Gas Experiment II (SAGE-II)

7.1 Introduction

The SAGE II (Stratospheric Aerosol and Gas Experiment II) sensor was launched into a 57 degree inclination orbit aboard the Earth Radiation Budget Satellite (ERBS) in October 1984. During each sunrise and sunset encountered by the orbiting spacecraft, the instrument used the solar occultation technique to measure attenuated solar radiation through the Earth's limb in seven channels centered at wavelengths ranging from 0.385 to 1.02 μm. The exo-atmospheric solar irradiance is also measured in each channel during each event for use as a reference in determining limb transmittances.

The transmittance measurements are inverted using the "onion-peeling" approach to yield 1-km vertical resolution profiles of aerosol extinction (at 0.385, 0.453, 0.525, and 1.02 μm), ozone, nitrogen dioxide, and water vapor. The focus of the measurements is on the lower and middle stratosphere, although retrieved aerosol, water vapor, and ozone profiles often extend well into the troposphere under non-volcanic and

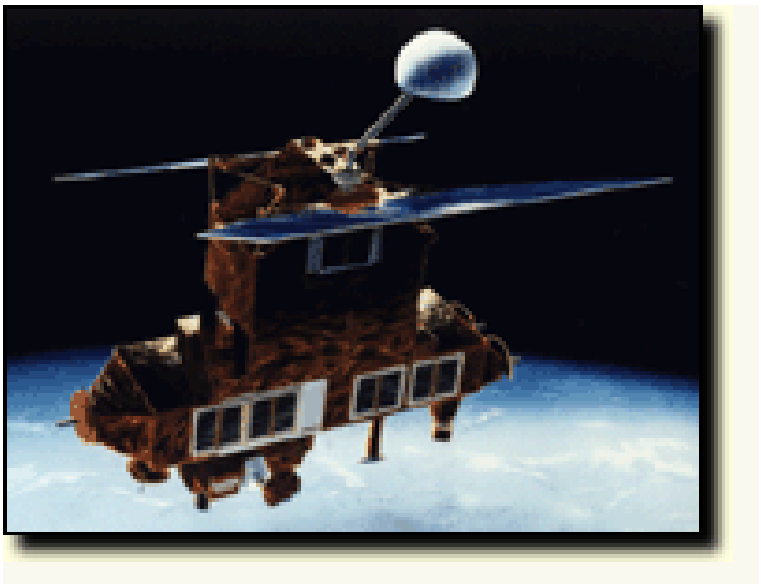

Figure 7.1: Earth Radiation Budget Satellite, adapted from NASA website

cloud-free conditions. SAGE II was preceded into orbit by sister instruments SAM II (Stratospheric Aerosol Measurement II)[44], which has been measuring 1.0 μm aerosol extinction in the polar regions since 1978, and SAGE I, which provided near global measurements of aerosol extinction (at 0.45 and 1.0 μm), ozone, and nitrogen dioxide from 1979-1981. Since the solar occultation technique is inherently self-calibrating, accurate estimates can be made of long-term trends in the retrieved atmospheric constituents to aid in assessing their role in global change.

7.2 Stratospheric aerosol

Stratospheric aerosols affect the atmospheric energy balance by scattering and absorbing solar and terrestrial radiation. They can also alter stratospheric chemical cycles by catalyzing heterogeneous reactions which markedly perturb odd nitrogen, chlorine and ozone levels. Since routine measurement of stratospheric aerosol began

in the late 1970's, aerosol has primarily originated from episodic injections of SO_2, a gaseous precursor to sulfate aerosol. Volcanic eruptions can inject a large amount of this gas into the stratosphere. For instance, the 1991 eruption of Mt. Pinatubo in the Philippines increase the total stratospheric aerosol mass by a factor of approximately 30 to about 30 Tg. Other noteworthy eruptions include Tambora (Indonesia) in 1815, Krakatau (Indonesia) in 1883, and El Chichon (Mexico) in 1982. Not all eruptions result in a significant impact on stratospheric aerosol levels. For instance, Mt. St. Helens (US) in 1980 and Nevado del Ruiz (Colombia) in 1985, which killed over big number of people, had only modest effects on the stratosphere [45].

The non-volcanic sources of aerosol include the transport of carbonyl sulfide (OCS), a product of biologic activity, from the lower atmosphere in the stratosphere where it is photochemically transformed into sulfate aerosol.

7.3 Theoretical back ground of aerosol parameter retrieval

The volume extinction coefficient β_λ which describes both scattering and absorption of light particles, is given by [46]

$$\beta(z,\lambda) = \int_0^\infty N(z) f(r) Q(r,\lambda,m) dr \tag{7.3.1}$$

where is the $Q(r,\lambda,m)$ Mie extinction efficiency, which is a function of size parameter $\frac{2\pi r}{\lambda}$ and the index of refraction m, and the size distribution N(z), which is the number of aerosol particles per unit volume of air. f(r) is usually described by lognormal

function with modal radius r_g and width σ

$$f(r) = \frac{1}{\sqrt{2\pi} r \ln \sigma} \exp(-\frac{(\ln \frac{r}{r_g})^2}{2 \ln^2 \sigma}) \tag{7.3.2}$$

The index of refraction m is a function of aerosol composition x, temperature T and wave length λ. The dependence of the index of refraction on temperature is given by

$$\frac{m^2 - 1}{(m^2 + 2)\rho} = constant \tag{7.3.3}$$

where ρ is the density of the sulfuric acid solution [47]. It is because generally accepted that stratospheric aerosol particles are primarily composed of a supercooled sulfuric acid and water solution, and is a function of both T and x. The aerosol parameter retrieval is carried out by inversion of Eq (7.3.1). The problem consists of replacing $\beta(z, \lambda)$ by a set of experimental data $\beta^e(z, \lambda)$ and finding the optimal corresponding values (N, r_g, σ). The problem can be simplified by eliminating the $N(z)$ variable, using the normalization

$$\beta_n = \frac{\beta(z; \lambda)}{\beta(z; \lambda_r)} \tag{7.3.4}$$

In our case, we chose the channel $\lambda = 1.020$ μm for the normalization of $\beta^e(z, \lambda)$ in to $\beta_n^e(z, \lambda)$ values. By using Eq (7.3.4), the inversion problem comes down to the inversion of

$$\beta_n(z, \lambda) = \frac{\int_0^\infty f(r) Q(r; \lambda) dr}{\int_0^\infty f(r) Q(r; \lambda_r) dr} \tag{7.3.5}$$

and can be solved by building look up table of theoretical values $\beta_n^t(\rho, \sigma; \lambda_i)$ using Eqs (7.3.2) and (7.3.5), for a set of value of ρ, σ chosen in the working ranges $[\rho_{min}, \rho_{max}]$ and $[\sigma_{min}, \sigma_{max}]$ spanning the solution domain. For each z values, a least square minimization is performed on the merit function

$$M(\rho, \sigma; z) = \Sigma_{i=1}^4 [\frac{\beta_n^e(z; \lambda_i) - \beta_n^t(\rho, \sigma; \lambda_i)}{\triangle \beta_n^e(z; \lambda_i)}]^2 \tag{7.3.6}$$

leading to the solution in ρ and σ. N is then retrieved by injecting β_e, ρ and σ in to Eq (7.3.1) using Eq (7.3.2). The extinction cross section $Q(r;\lambda)$, in Eq (7.3.5), is computed from the Mie theory which describes the extinction of light by spherical particles. When the particle size on the same order of magnitude as the wavelength, the expression obtained for $Q(r;\lambda)$ is a rather complex function of ρ and σ. On the contrary, when the particle size is small compared to λ, this function simplifies into an expression which only depends on the wavelength. In this case corresponding to the Rayleigh limit of scattering, the inversion algorithm is unable to discriminate the structure of particle population.

Chapter 8

Results and discussions

The mixing ratio of methane shown in Fig 8.1 over equatorial latitude is obtained by averaging all FTIR measurements available for the given time. As shown in Fig 8.1, methane is highly concentrated over the troposphere and lower stratosphere of tropical latitude. We find mixing ratio is uniformly distributed over the latitude 20^o north and 20^o south for lower atmospheric region indirectly supporting the quality of our retrieval. But south of 20^0 large pick of the VMR of this gas is observed, which might be attributed to a number of factors ranging from poor quality spectra to apriori VMR used. We can certainly conclude, the observed feature is an artifact since CH_4 VMR of this magnitude can not be observed in stratosphere under any dynamic or chemistry. In line with its sink nature and its oxidation property over the regions of the atmosphere, the volume mixing ratio is decreasing with height over most latitudes with the above exception, which is also another way that assures a good quality of the retrieval result.

Consider Fig 8.2, where there is no strong variation in total column (number of molecules per square centimeter, or the optical density of methane over the region of

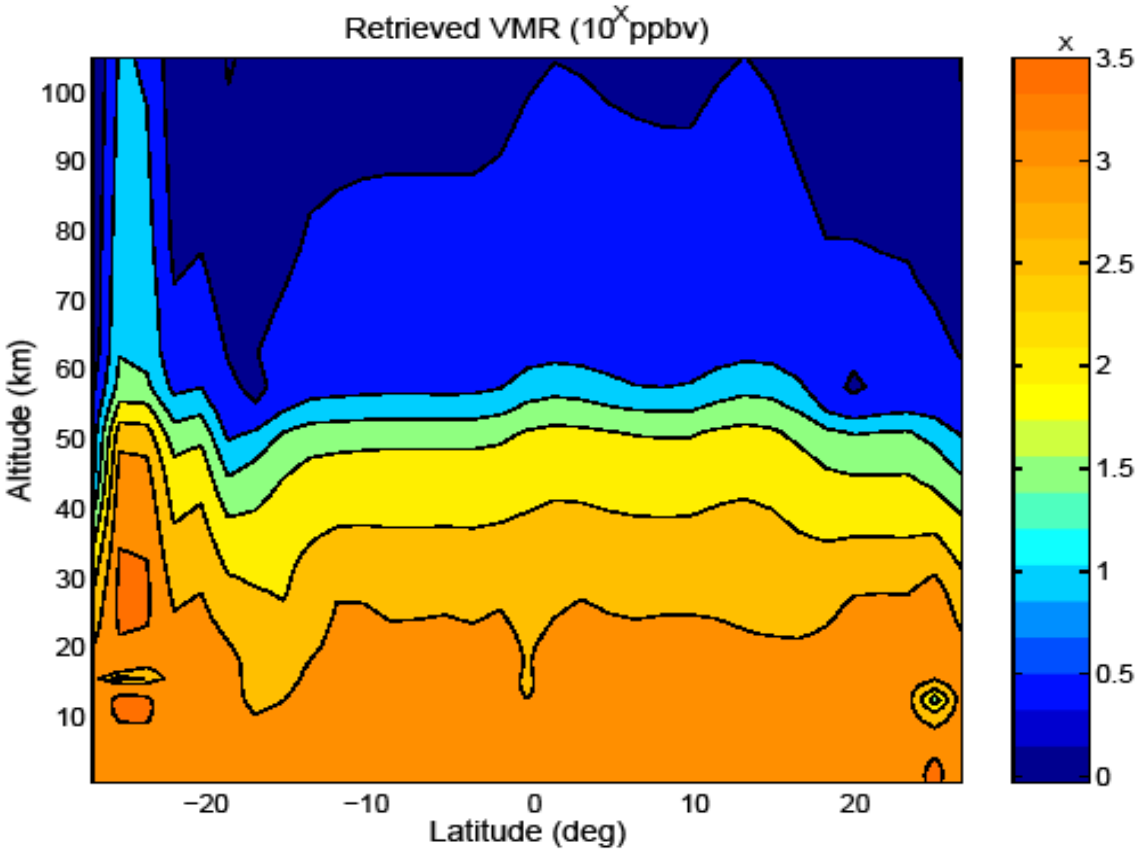

Figure 8.1: Retrieved methane VMR over equatorial latitudes from 1996 spectral records of FTIR spectrometery

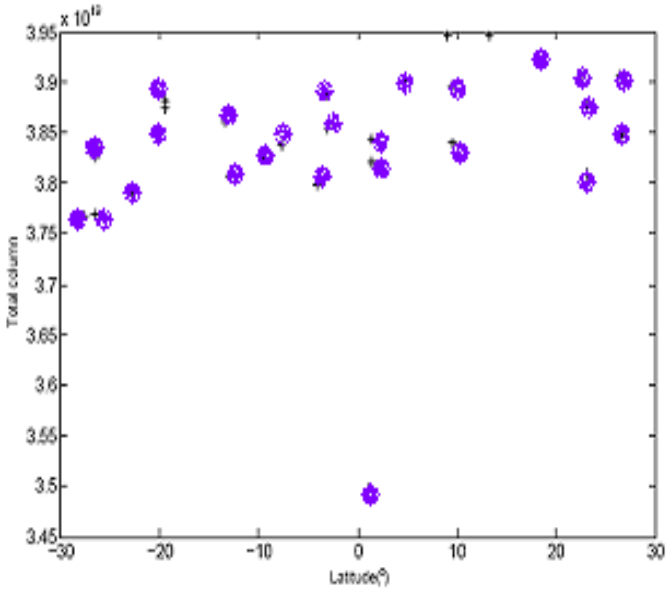

Figure 8.2: The total column measurement

study in units of molecules per square centimeter). This nearly uniform distribution indicates the balance of the air mass entering and leaving the column in consideration. It may also indicate the chemistry of methane in the region, which depends on the strength of the source and sink though it has insignificant influence since methane has got a very long lifetime in the troposphere. The above observed equilibrium advection condition tells us the good meteorological phenomena of the time of spectral record over the region. Thus, we can say that the FTIR spectral record was insignificantly affected by the dynamics of air, which gave total column characterized by uniform distribution thereby witnessing the good quality of retrieved VMR.

Fig 8.3 provides us with the information about the signals of the retrieved state for the region covering our study. The degree of freedom we obtained for the retrieved VMR is 2, which tells us the sensitivity of methane in the region. As a consequence, we find

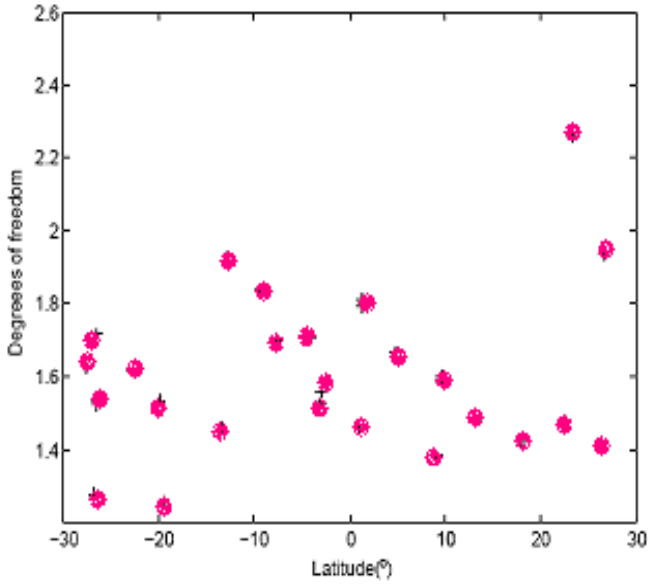

Figure 8.3: The degrees of freedom

that methane is highly sensitive in the regions from 10^0 south to 20^0 latitudes north. But also less sensitive in the region covering latitudes from 20^0 south to 10^0 south. But, we observed unhealthy sensitivity of methane over the region south of 20^0. The information from aforementioned highly sensitive region of methane provides good reliability of information about the retrieved parameter and the insensitive regions provide unreliable information that may be resulted from poor a prior information and poor signal records.

8.1 Methane VMR Validation

The retrieved volume mixing ratio obtained from our ground-based FTIR measurements have been compared with the retrieved volume mixing ratio obtained from the Halogen Occultation Experiment (HALOE) satellite.

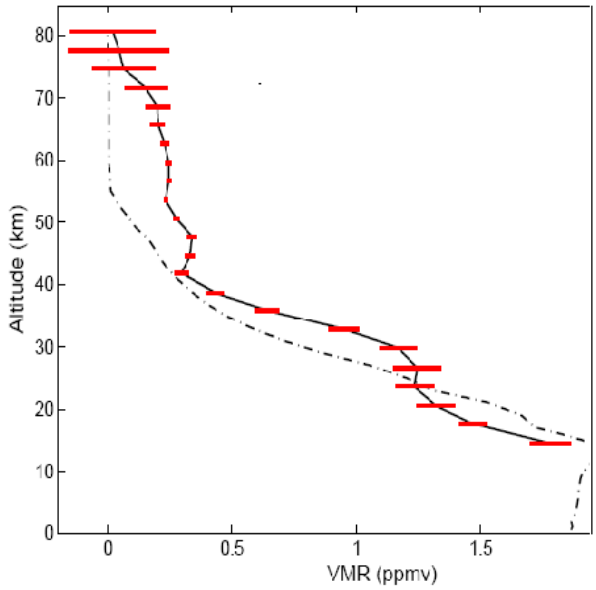

Figure 8.4: The comparison of the retrieved VMR from the spectra of HALOE and FTIR

The Halogen Occultation Experiment (HALOE) was launched on the Upper Atmosphere Research Satellite (UARS) spacecraft September 12, 1991. It began science observations October 11, 1991. The experiment uses solar occultation to measure vertical profiles of O_3, HCl, HF, CH_4, H_2O, NO, NO_2, aerosol extinction at 4 infrared wavelength, and temperature versus pressure with an instantaneous vertical field of view of 1.6 km at the Earth's limb. Latitudinal coverage is from 80 S to 80 N over the course of 1 year and includes extensive observations of the Antarctic region during spring. The altitude range of the measurements extends from about 15 km to 60-130 km, depending on the species.

The criteria we set for validation is spatial collocation between the records of the two instruments. Hence, the spatial collocation we used is $10 - 15^o$ difference in latitude

and longitude. Then the comparison result is shown in Fig 8.4, where the broken line indicates the volume mixing ratio of methane retrieved from FTIR while the solid line indicates the retrieved volume mixing ratio of methane from HALOE record. According to the Fig 8.4 we find that the retrieved data are fairly in agreement from 14 km to 40 km. But we observed big discrepancy between the data from 40 km to 70 km. And again the good agreement between the data from 70 km to 80 km. The discrepancy is mainly due to less than perfect spatial and temporal collocation. But temporal mismatch has weak effect on CH_4 in troposphere since it is a long lived in troposphere. However, its impact in the stratosphere might be important due to photolysis. Since the data obtained from the HALOE does not include for the region bellow 14 Km we are not able to compare the data of that region. But for the region covered by both instrument we find good agreement indicating the good quality of the retrieved VMR of methane from FTIR.

8.2 Aerosol climatology

To study temporal variations and spatial distribution of stratospheric aerosols SAGE II data can be used to derive temporally averaged zonal mean profiles of extinction coefficient. Since it provided a long range of information, the aerosol climatology obtained from it will help us validate the mobile lidar system of NLC-CSIR.

The 57 degrees inclined orbit of the ERBS spacecraft evenly distributes the SAGE II measurements every 24 degrees of longitude along a slowly shifting latitude circle. The SAGE II instrument vertically scans the limb of the atmosphere during spacecraft sunsets and sunrises (fifteen sunsets and fifteen sunrises) each day. The instrument

had approximately 30 measurement opportunities each day. Near-global coverage 80^o S to 80^o N was achieved over time spans of about 1 month. The instrument mission was terminated on 8 September 2005.

For clear geographical observation of the trend of aerosols we classified Africa in to four regions based on latitudinal and longitudinal locations as follows:

1. Northern Africa (-20^0)-(55^0) Longitude and (15^0)- (40^0) latitude
2. Southern Africa (10^0)-(40^0) Longitude and (-15^0)-(-40^0) latitude
3. Western Africa (-20^0)-(22.5^0) Longitude and (-15^0)-(15^0) latitude
4. Eastern Africa (22.5^0)-(55^0) Longitude and $(-15^0) - (15^0)$ latitude

and we used codes written in matlab programming to filter out corresponding data and to draw figures.

The Monthly mean aerosol extinction profile of northern Africa revealing the aerosol concentration of the region is shown in Fig 8.5. According to the figure, large tropospheric extinction concentration is observed from April to may, which are the summer months of the region indicating large aerosol concentration. And also, the lower tropospheric (3 to 7 km) aerosol extinction concentration is observed for the time from July to September. An intense view on the figure around three kilometers on October is showing large aerosol extinction concentration on this particular time and position. But from November to March very low aerosols extinction profile is observed.

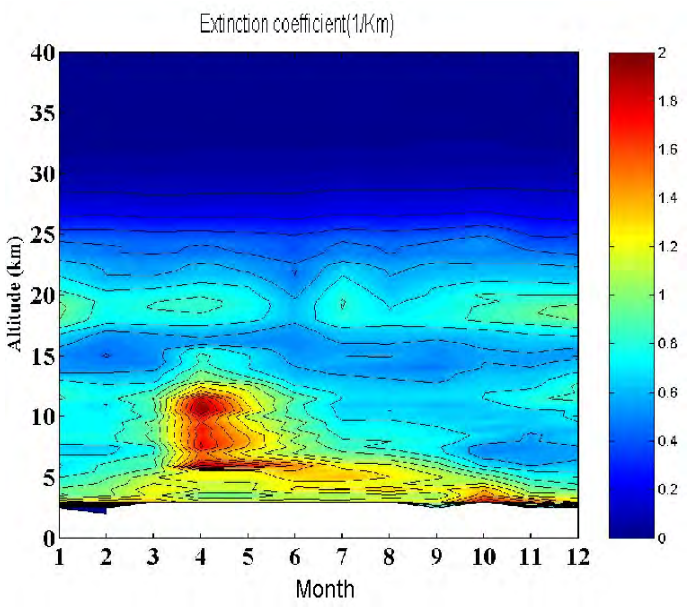

Figure 8.5: Monthly variation of aerosol extinction coefficient for Northern region of Africa, for $\lambda = 525\mu$m

Fig 8.6 shows the month to month mean aerosol extinction profile of southern Africa. It indicates that large accumulation of aerosols exist in the lower tropospheric (3 to 5 km) region from January to April. But the same region has got very little aerosols distribution from May to July except particular concentration view of aerosol around 13 km on July. Vertically (from 3 to 13 km) extended pronounced aerosol distribution is observed since August to September.

The monthly mean aerosol profile of Western region from the entire record is too few to explicitly discuss the aerosol climatology of the region. So we completely ignored it.

Likewise Fig 8.7 shows the month to month mean aerosol extinction coefficient distribution of eastern Africa. It clearly showed the pronounced aerosol concentration

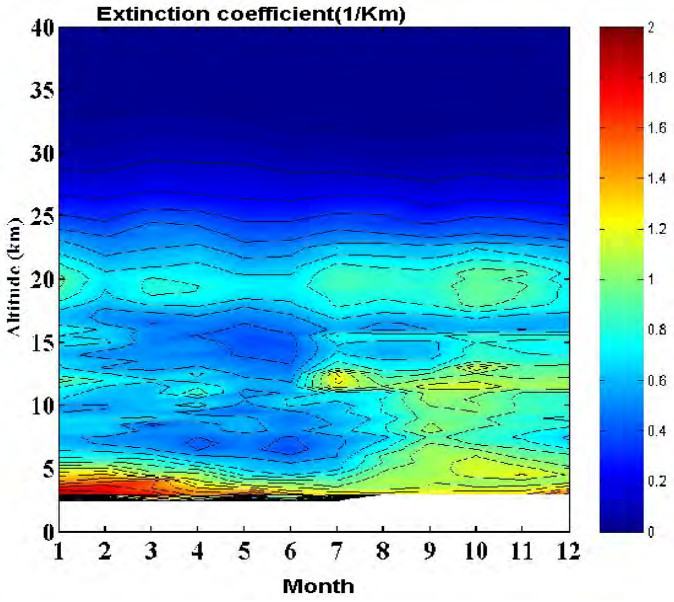

Figure 8.6: Monthly variation of aerosol extinction coefficient for Southern Region of Africa, for $\lambda = 525\mu$m

from 3 to 6 Km and 14 to 17 Km for the time from January to June. But from June to July low aerosol concentration is observed in the troposphere but large concentration in the lower stratosphere. And also, from July to December very large aerosol concentration in the lower tropospheric, and lower and middle stratospheric region is observed. And also the biggest aerosol concentration is observed for the month of April around 15Km. Unlike the aforementioned regions very large aerosol concentration is seen in this region.

The pronounced concentration of aerosols over the atmospheric region of eastern Africa may be resulted from an active volcanic eruptions of the region, which are continuously ejecting aerosols to the atmosphere. For example, a number of active volcanic eruptions are occurring even recently in eastern Africa. According, to the

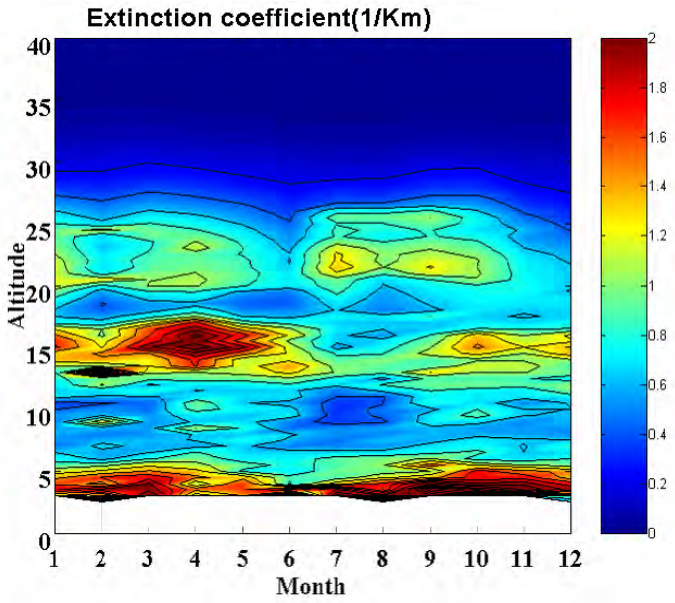

Figure 8.7: Monthly variation of aerosol extinction coefficient for Eastern region of Africa $\lambda = 525\mu$m

NEWS of 'geology. com (October 7, 2008, November 21, 2008) and MODIS; The Advanced Space borne Thermal Emission and Reflection Radiometer (ASTER) on NASA's Terra satellite captured that the volcano on the Red Sea island of Jabal al-Tair off the coast of Yemen is still erupting, and in Ethiopia's Afar region as well. So, such kind of eruptions might have been continuously ejecting particulate materials contributing such increase in the aerosol concentration in the region.

It is clear that the dynamics and chemistry of the atmosphere play a great role in the duration of aerosols over the atmosphere. Thus, it is apparent that the deposition rate of stratospheric aerosols is weak so that ruminants of big eruptions such as the Pinatubo might have remained in the stratosphere after injection in the atmosphere. And also the Philippine volcano Mount Pinatubo (15.1^o N, 120.4^o E) erupted violently

in mid-June 1991, emitting massive plumes that penetrated well in to the stratosphere, reaching altitude as high as 40 km. Due to the atmospheric transport of aerosols from those sources might have contributed to the concentration of aerosols of the nearest regions, Northern and Eastern Africa.

8.3 Lidar Validation with SAGE-II aerosol data

Introduction to lidar remote sensing

A lidar is an active remote sensing instrument, meaning that it transmits electromagnetic radiation and measures the radiation that is scattered back (backscatter) to a receiver after interacting with various constituents of the atmosphere. Lidars use radiation in the ultraviolet, visible or infrared region of the electromagnetic spectrum. Different types of physical processes in the atmosphere are related to different types of light scattering. Choosing different types of scattering processes allows atmospheric composition, temperature and wind to be measured.

The basis for lidar remote sensing lies in the interaction of light with gas molecules and particulate matter in suspension in the atmosphere (aerosols). More particularly, a lidar uses a laser (emitter) to send a pulse of light into the atmosphere and a telescope (receiver) to measure the intensity scattered back (backscattered) to the lidar. By measuring the scattering and attenuation experienced by the incident pulse of light, one can investigate the properties of the scatterers (concentration of gaseous species, aerosol distribution and optical properties, cloud height) located in the atmosphere. The light scattered back to the detector comes from various distances, or ranges, with respect to the lidar. Because the light takes longer to return to the

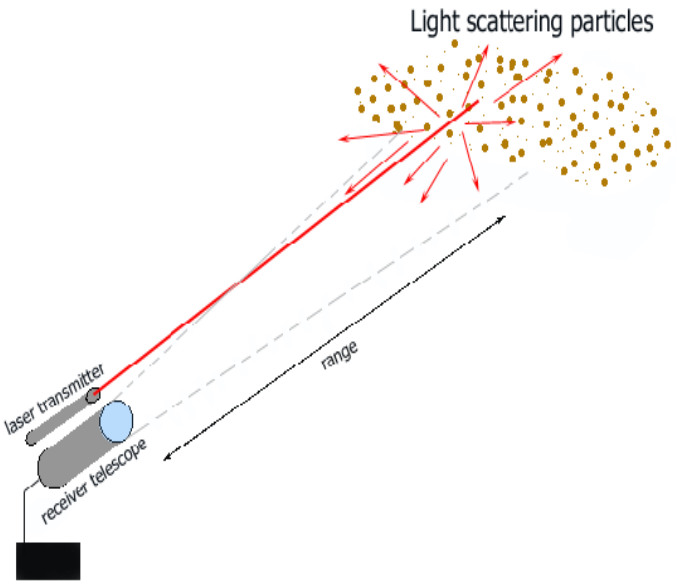

Figure 8.8: Lidar principle

receiver from targets located farther away, the time delay of the return is converted into a distance (range) between the scatterers and the lidar, since the speed of light is a well-known quantity. By pointing the laser beam in various directions and at various angles with respect to the ground surface (scanning), a ground-based lidar system can gather information about the three-dimensional distribution of aerosols in the atmosphere.

The backscattered radiation detected by a lidar is described by the lidar equation. In general terms, the received power is expressed as a function of range R. For a simple backscatter lidar (measuring backscattered light at the same wavelength as the laser wavelength), the lidar equation is written as [48]:

$$P_r(\lambda_L = \frac{Ch}{R^2 2} O(R) \frac{\beta(\lambda_L, R)}{4\pi} \exp(\int_0^R \kappa_e(\lambda_L, r' dr') \tag{8.3.1}$$

where P_r is the power returned to the lidar at the laser wavelength λ_L, C is the lidar constant, R is the range, $h = ct_p$ where t_p is the pulse duration and c the speed of light. The term O(R) describes the overlap between the laser beam and the receiver field of view. The term is equal to 1 for ranges where there is complete overlap of the laser beam and the receiver field of view. Here, $\beta(\lambda_L, R)$ and $\kappa_e(\lambda_L, r^{'}dr^{'})$ are the combined aerosol and molecular backscatter and extinction coefficients respectively, at the laser wavelength. The combined backscattering coefficient can be re-written as the sum of molecular and aerosol backscattering $\beta(\lambda_L, R) = \beta^a(\lambda_L, R) + \beta^m(\lambda_L, R)$. The aerosol scattering ratio (ASR) is defined as the ratio of the total (aerosol + molecular) backscattering to the molecular backscattering:

$$ASR = \frac{\beta^a(\lambda_L, R) + \beta^m(\lambda_L, R)}{\beta^m(\lambda_L, R)} \tag{8.3.2}$$

where β^a is the aerosol backscattering coefficient and $\beta^m(\lambda_L, R)$ is the molecular (Rayleigh) backscattering coefficient. The elastic return at the laser wavelength depends on both the Rayleigh and Mie (molecular and aerosol) scattering.

The molecular backscattering $\beta^m(\lambda_L, R)$ can be estimated using air density profiles obtained from radiosondes or from a co-located ground-based Atmospheric Emitted Radiance Interferometer (AERI). Then, the ASR profile is used in conjunction with the molecular (Rayleigh) backscattering profile to obtain the corresponding aerosol backscattering β^a profile.

Lidar Validation

The backscatter and extinction profile were derived from the lidar whose system description given [49] data and is being presented here. The obtained results are further

compared and validated using ground based and satellite borne instruments. Fig 8.9 presents the height profile of extinction coefficient derived from the lidar data taken during the nights of 25 February 2008. The profiles are overlapped by Stratosphere Aerosol Gas Experiment (SAGE) extinction data at 525nm collected over southern Africa regions. The SAGE monthly mean extinction profiles obtained for each month are compared. The mean profiles should serve as background aerosol information over Southern Africa and has been calculated using 21 years of data sets. The extinction profile derived from LIDAR and SAGE-II is closer in agreement with trend and magnitude. The LIDAR profile has been terminated above 10 km due to thick cloud passage; otherwise, one can also notify the boundary layer peak at 3 km which is considered to be an important parameter for model and atmosphere mixing (including pollutants). The presence of a cloud results in a sharp enhancement in the extinction and backscatter co-efficient to a high value making the detection quite unambiguous. The major advantage of LIDAR data is to detect clouds and determine their spatial and temporal characteristics.

During 21:09-21:30, the scattering ratio is found to increase sharply to a value of about 6 at a height around 13km representing a cloud. The thickness of the cloud, represented by full-width at half maximum of the enhancement peak, is of the order of 1km. In the absence of cloud, the peak scattering ratio is only of the order 1.2 representing aerosol concentration peak at about 18 Km as observed during 22:59-23:26. The bottom pair of panels shows the evolution of the cloud during 00:25-01:40 at the same height level as observed earlier. The upgradation of lidar into dual polarization

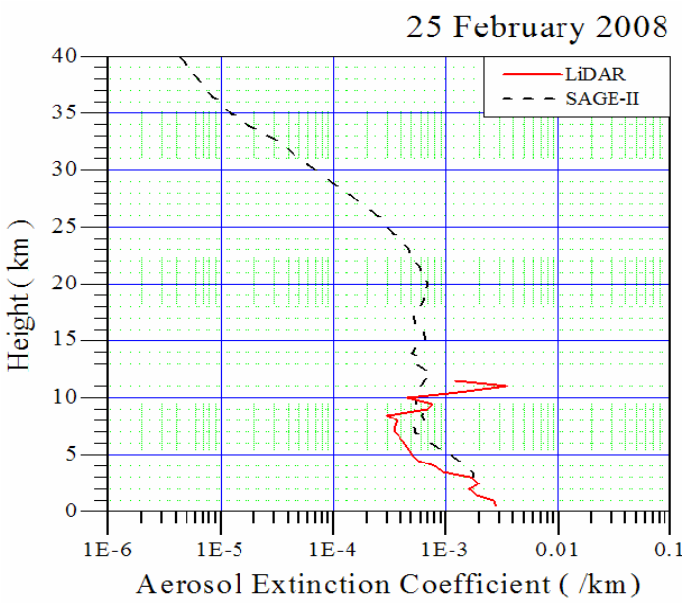

Figure 8.9: Aerosol extinction profiles observed on the nights of 25 February 2008.

(Co-and Cross Polarization) measurements of the backscattered signal allows to determine the relative concentrations of water and ice in the clouds.

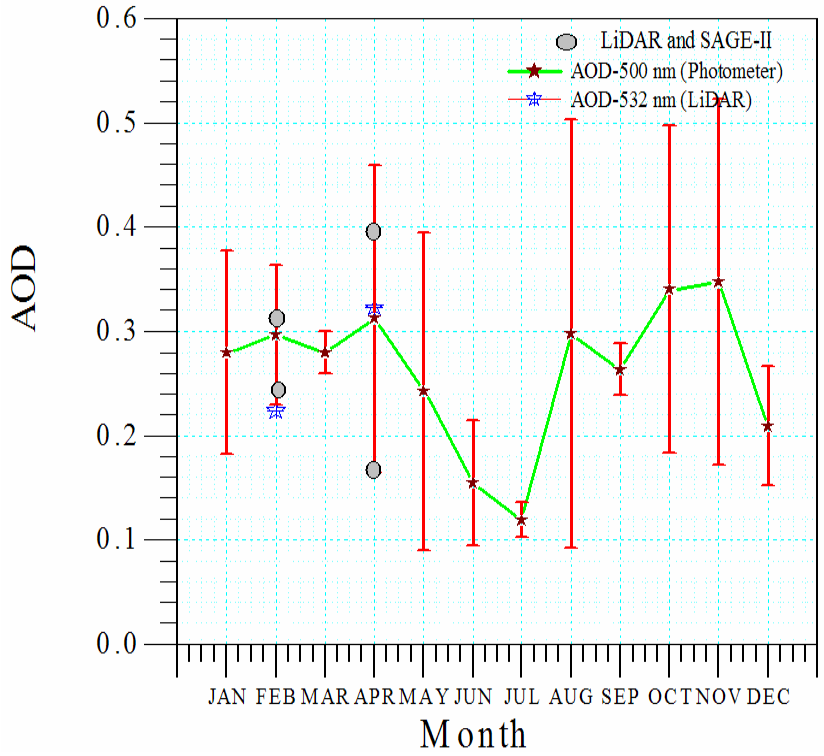

Figure 8.10: Optical depth derived from LIDAR and SAGE-II comparison with AERONET.

Chapter 9

Conclusions

By using the retrieval technique and the spectral records of ground based FTIR, we find that the VMR of methane concentrated over the troposphere and lower stratosphere of the tropical latitudes. The uniform distribution of methane in the troposphere, which is the property of source gases is also observed over this region in addition to the noticeable decrease of its concentration with altitude. Moreover, by using the spectra of ground based FTIR spectroscopy we observed the expected features of methane supporting the good quality of retrieved VMR. Thus we can conclude that ground based FTIR spectroscopy is a very useful technique to derive the VMR of trace gases.

The technique we used helped us to retrieve the VMR of methane over the mentioned region with 2 independent pieces of information. The obtained DOFs clearly indicated the region of information source for methane signal. Moreover, the total column of methane has indicated the good dynamic condition during the time of spectral measurement thereby reveling the good quality of retrieved methane VMR. Further work is needed to continually assess the volume mixing ratio of methane.

Long-term observations from satellite remote sensors, complemented by lidar and in situ measurements, have significantly improved our understanding of the climatology of stratospheric and troposheric aerosols over the last decades. The records of aerosols extinction from the SAGE-II, which spans from 1984-2004 has shown picture of the climatology of aerosols over the region of Africa. Among four wave lengths through which the satellite provides the aerosol profile we used the 525 μm channel, which clearly provided the required information.

From the study we have seen that the SAGE II instrument provided a plenty of information about the aerosol distribution over the atmospheric regions of Africa. Consequently, a good picture of climatology of Africa is made via extinction coefficient profiles of very long records of the data. The very large cluster of the stratospheric aerosols observed over the Eastern and Northern region might have come from the two massive volcanic eruptions which occurred before the launch and during the operational time of SAGE II, El Chichon (1982) and Mount Pinatubo (1991). In addition, a number of volcanic eruptions occurs in eastern region so that we find that the aerosol concentration is observed higher than the other regions. To see the effects imposed on climate by these cloud of aerosol over stratosphere and troposphere future work should focus on calculating radiative forcing. In addition, efforts has to made to find the dominant species of aerosols in the atmosphere of the region so as to have a good picture of the aerosols distribution.

Finally it is found that the extinction profile obtained by LIDAR is in agreement with that obtained by the SAGE-II satellite.

Bibliography

[1] Elachi, C. and Van, Z. J. *Introduction to the Physics and Techniques of Remote Sensing*, 2nd edition Wiley-Interscience, USA 2006.

[2] Lutgens, F. K. and Tarbuck, E. J. *An Introduction to Meteorology*, 8 edition, Prentice Hall 2000.

[3] Liou, K. N. *An Introduction to Atmospheric Radiation* , 8 edition, Elsevier Science 2002.

[4] IPCC(2001), Climate Change 2001: *The Scientific Basis. Contribution of Working Group I to the Third Assessment Report of the Intergoveronmental Panel on Climate Change, 881 pp.,* Cmbridge, United Kingdom and New York, NY, USA

[5] Barrow, M. G. *Introduction to Molecular Spectroscopy*, McGraw-Hill, United States of America, 1962.

[6] Rinsland, C. P., Goldman, A. Connor, B. J., Stepen, T. M., Jones, N. B., Wood, S. W., Murcray, F. J. David, S. J., Blatherwick, R. D., Zander, R., Mahieu, E. and Demoulin, P. *"Correlation relationships of stratospheric molecular constituents from high spectral resolution, ground-based infrared absorption spectra".* J. Geophys. Res., 105, 14637 - 14652, 2000.

[7] Rothman, L. S, *The HITRAN molecular spectroscopic database and HAWKS (HITRAN Atmospheric Workstation)*: 1996 edition, J. quant. Spectroscopic and Radiative transfer, 60, 665-710, 1998 Atmos. Chem. Phys., 6. 1953-1976, 2006.

[8] Rao, K. N. and A. Weber, *Spectroscopy of the Earth's atmospher and Interstellar Medium*, 2nd ed., Elsevier, New york, 1992

[9] IPCC, Climate Change 1995: *Line-by-line calculation of atmospheric fluxes and cooling rates, 2, application to carbon-dioxide, ozone, methane, nitrous- oxide and the halocarbons*, J. Geophys. Res., 100, 16, 519-16, 535, 1995.

[10] Dlugokencky, E. J., Steele, L. P., Lang, P. M. and Masarie, K. A. 1994. *The growth rate and distribution of atmospheric methane.* J. Geophys. Res., 99, 17021-17043.

[11] Finlayson-Pitt, B. J, *Atmospheric Chemistry: FundamentalsAnd Experimental Techniques*, Wiley-Interscience, United States of America 1984

[12] Jacobson, Z. M. *Fundamentals of Atmospheric Modeling*, 2nd edition, Cambridge University, 2005.

[13] Wassmann, R. Neue, Lantin, H. U. Javellana, Diego, R. S., Lignes, M. J. R. V. E. Hoffmann, H. Papen, H. Rennenberg, H. *Methane emissions from rained rice fields*, Zeitschriftenaufsatz Vol. 229. no. 4720, pp. 1386 - 1388, DOI: 10.1126/science. 229. 4720. 1386

[14] Khalila, M. A. K. and Rasmussen, R. A. 1984, *Atmospheric methane: Trends over the last 10, 000 years.* Elsevier. 2445-2452.

[15] Stauffer, B., Fischer, G., Neftel, A. and Oeschger, H. Increase of Atmospheric Methane Recorded in Antarctic Ice Core. Science 27 September 1985: Vol. 229. no. 4720, pp.1386-1388, DOI: 10.1126/science. 229. 4720.1386

[16] Graedela, T.E. and Mcrae, J. E. *Total organic component data: A study of urban atmospheric patterns and trends.* Elsevier. Volume 16, Issue 5, 1982, Pages 1119-1132.

[17] Dickinson, E. R. and Cicerone, J. R. *Furure global warming from atmospheric trace gases.* Nature(London), 319(9), 109-118, 1986.

[18] Cicerone, J. R. and Oremland, S. R. *Biogeochemical aspects of atmospheric methane.* J. Geophys. Res., 83, 947-952, 1978

[19] Levine, I. N. *Molecular Spectroscopy.* A Wiley-Interscience Publication, United States of America, 1975.

[20] Forschungszentrum Karlsuhe GmbH *The Karlsruhe Optimized and Precse Radiative transfer Algorithm.* Karlsruhe, 2000.

[21] Craig, A. R. *The Upper Atmosphere: Meteorology and Physics*, New York, 1965

[22] Andrews, D. G. *An introduction to Atmospheric Physics.* Cambridge University Press, United States of America, 2000.

[23] Roders, C. D. *Inverse methods for Atmospheric sounding; Theory and Practice*, vol.2, World Sientific Publishing, Singapore, 2000.

[24] Houghton, J., *The Physics of Atmospheres,3rd ed.,*, Cambidge University Press, New York, 2002

[25] Arndt Meier, Geoffrey C. Toon, Curtis P. Rinsland, Aaron Goldman and Frank Hase *Spectroscopic Atlas of Atmospheric Microwindows in the Middle Infra-Red*, 2nd edition, Swedish Institute of Space Physics, Kiruna, Sweden, IRF Technical Report 048 April 2004.

[26] Backus, G. and Gilbert, F *Uniqueness in the inversion of inaccurate gross earth data*, Philos. Trans. Roy. Soc. London, Ser A, 123192, 1970

[27] Aitken, J. *On the number of dust particles in the atmosphere*, Nature 37, 428-430, 1888.

[28] Mie, G. *Determining Pigment Optical Properties for Use in the Mie and Many-Flux Theories*, Ann. Phys. 330, 377445, 1908

[29] Nolan, P. J. and Doherty, D. J. *Size and charge distribution of atmospheric condensation nuclei.*, Proc. Roy. Irish Acad., A 53, 163-179, 1950.

[30] Chamberlain, A. C. and Dyson, E. D. *Influence of radioactive aerosol and biological parameters of inhaled radon progeny on human lung dose* , Br. J Radiol. 29, 317 1956.

[31] d'Almeida, G. A. Koepke, P. Shettle, E. P *Atmospheric Aerosols, Global Climatology and Radiative Characteristics*, Deepak Publishing: Hampton, VA, 1991.

[32] Junge, C. E. *The Properties and Climate of Atmospheric Haze*, Ann. Meteor Beiheft 1-55 1952a.

[33] Junge, C. E. *The Properties and Climate of Atmospheric Haze*, Ber. Deutsch, Wett, D. U. S. Zone 35, 261 1952b.

[34] Savoie D. L., and Prospero, J. M. *Particle size distribution of nitrate and sulfate in marine atmosphere.*, Geophys. Res. Lett., 9. 1207-1210, 1982.

[35] WoodCock, A. H., and Gifford, M. M. *Sampling atmospheric sea-salt nuclie over the ocean.*; J. Marine Res, 8, 177-197, 1949

[36] Cour, P. and Van Campo, M. *Prvisions de rcoltes partir de l'analyse du contenu pollinique de l'atmosphre.*; C. R, Acad. Sc. Park, 290: 1043-1046.

[37] Junge, C. E. *Air chemistry and radioactivity*; New York: Academic press, 1963

[38] Blanchard, D. C. and Woodcock, A. H.*The production, concentration, and vertical distribution of the seasalt aerosol*, Ann. N. Y. Acad. Sci. 330-347 1980.

[39] d'Almeida, G. A. and Schtz, L. *Number, mass and volume distributions of mineral aerosols and soils of the Sahara.*J. Clim. Appl. Meteorol. 22: 233-243, 1983.

[40] Isral, H. and Isral, G. W. *Trace Elements In the Atmosphere*, Ann-Arbor Science Publisher, USA 1974.

[41] Labitzke, K. and McCormick, M. P. *Stratospheric temperature increases dueto pinaubo aerosols*, Geophysical Research letters, Vol. 19, No. 2, Pages 207210, 1992

[42] Andres, R. and Kasgnoc, A. *A time-averaged inventory of aerial volcanic sulfur emissions.*, Geophysical Research letters, No. 103, Pages 25,251-25,261,1998

[43] http://eosweb.larc.nasa.gov/GUIDE/$campaign\_documents/sage1\_project.html$

[44] http://oea.larc.nasa.gov/PAIS/SAGE.html

[45] http://en.wikipedia.org/wiki/1980 $\_eruption\_of\_Mount\_St.\_Helens$

[46] Bingen, C. Fussen, D. Vanhellemont, F. *A global climatology of stratospheric aerosols using SAGE II: toward a systematic characterization of the aerosol evolution.* Elsevier. Advances in Space Research volume 34, Issue 8, 2004, Pages 1763-1767.

[47] Yue, G, K. McCormick, M. P. and Chu, W. P. *Retrieval of Composition and Size Distribution of Stratospheric Aerosols with the SAGE II Satellite Experiment.* Journal of Atmospheric and Oceanic Technology. Volume 3, Issue 3, September 1986, Pages 371-380.

[48] http://www.rap.ucar.edu/staff/tardif/CUprojects/ATOC5235/lidar_remote_sensing.htm

[49] www.csir.co.za/lasers/docs/system.